Spring 5-2020

Design and Validation of a Dynamic Pressure-Based Loading Device and 3D Strain Tracking Protocol for Ventral Hernia Modeling

Griffin Kivitz
Washington University in St. Louis

Washington University in St. Louis

McKelvey School of Engineering

Department of Mechanical Engineering

Thesis Examination Committee:

Dr. Spencer Lake

Dr. Jeffrey Blatnik, MD

Dr. Jessica Wagenseil

Design and Validation of a Dynamic Pressure-Based Loading Device and 3D Strain Tracking Protocol for Ventral Hernia Modeling

Griffin Joseph Kivitz

A thesis presented to the McKelvey School of Engineering of Washington University in St. Louis in partial fulfillment of the requirements for the degree of Master of Science

May 2020

St. Louis, Missouri

Dedicated to my parents and brother for

their unconditional love and support

Acknowledgements

I would like to thank the McKelvey School of Engineering at Washington University in St. Louis for my invaluable education and mentorship. Specifically, I want to mention Dr. Spencer Lake for his support and interest in both my academic and personal life. Dr. Lake welcomed me into his lab three years ago; the research I participated in and the relationships I built were more than enough to convince me to continue my research with him and shape my education around a newfound career goal of doing research and development for a medical device company. I also want to mention Alex Reiter, the PhD. Candidate that I worked with as an undergraduate student in the lab. Alex was the finest mentor I could ask for, and has had one of the biggest impacts on my life at WashU. He was, and still is, my role model in intuition, drive, and character. I want to thank Dr. Jeffrey Blatnik for his guidance and insight throughout this project, and Leanne Iannucci for her work in developing, troubleshooting, and implementing the strain tracking protocol. Lastly, I want to thank Ryan Castile for his interest and recommendations throughout the duration of this project. I am truly grateful for my time in the Musculoskeletal Soft Tissue Laboratory and the relationships I have built with the lab members.

Table of Contents

List of Tables

List of Figures

Abstract

Design and Validation of a Dynamic Pressure-Based Loading Device and 3D Strain Tracking Protocol for Ventral Hernia Modeling

By

Griffin Joseph Kivitz

Master of Science in Mechanical Engineering

Washington University in St. Louis, 2020

Research Advisor: Professor Spencer Lake

It is estimated that 350,000-500,000 ventral hernia repair surgeries are performed each year in the United States[1]. While the long-term recurrence rate of ventral hernia repairs is not yet known, when tissues are exposed to the trauma of surgery, there is always the chance of recurrence[1]. Commonly used *ex vivo* testing methods for determining the mechanical properties of the abdominal wall and biomaterials for hernia repair consist primarily of uniaxial and biaxial testing, which are not physiologically relevant loading environments[2]. The need for a testing device that can exert physiologically relevant loads *ex vivo* to an abdominal wall is crucial for the development of more effective repair strategies and products.

After abdominal hernia repairs, coughing poses a major threat to the structural integrity of the repair site. During a cough, the intra-abdominal pressure (IAP) can rise as high as 2.5 psi, compared to the normal IAP of approximately 0.1-0.2 psi[3]. The goal of this project was to design a testing device that could apply and measure a representative coughing force applied to an *ex vivo* porcine abdominal wall, and develop a strain tracking protocol to track three-dimensional abdominal deformation throughout the duration of the cough.

The constructed device was successful in applying a physiologically relevant force to a porcine abdominal wall, and subsequently decreasing the force back to a normal IAP in less than 2 seconds. The maximum force of the cough could be easily controlled using the Arduino controller, which makes the device robust enough to explore the effects of a range of pressures. By recording a video of the abdominal wall using a 3D camera during the application of a cough, we were able to successfully track the deformation of the tissue in three-dimensions with an acceptable level of accuracy. The design and validation of this testing method will pave the way for a variety of experiments that will provide greater insight into the mechanical behavior of the abdominal wall and the effectiveness of various repair strategies and products on restoring native tissue function.

Chapter 1: Introduction

Background

It is estimated that 350,000-500,000 ventral hernia repair surgeries are performed each year in the United States. While the long-term recurrence rate of ventral hernia repairs is not yet known, when tissues are exposed to the trauma of surgery, there is always the chance of recurrence[1]. A ventral hernia refers to any protrusion of intestine or other tissue through a weakness in the abdominal wall[4]. Following a ventral hernia repair, the repair site is fragile and susceptible to wound dehiscence. Coughing, which results in a sudden increase in intra-abdominal pressure (IAP), poses a serious threat to the structural integrity of the wound site. During coughing, the IAP can rise as high at 127 mmHg[3] (~2.5psi.) compared to the normal post-operative IAP of 3-15 mmHg[5] (0.058-0.29psi).

The majority of research on the mechanical properties of abdominal tissue and hernia repair materials has been limited by the lack of a physiologically relevant loading environment. Studies have shown the anisotropy of abdominal tissue and mesh products through uniaxial and biaxial testing, but neither of these loading environments are representative of the forces experienced by the abdominal wall *in vivo*[2]. However, it is important to note the work of two groups that have investigated hernia repair strategies in a physiologically relevant manner.

Dr. Simms' group constructed a device to model hernia formation in a porcine abdominal wall. Their device consists of a rectangular box containing an oversized balloon connected to a compressed air network capable of controlling air pressure up to 150mmHg. The top of the box has a radius of curvature of 200mm to mimic the circumferential curvature of the abdomen *in vivo*. The porcine abdominal wall is laid over the top of the box and balloon and fixed in place with a lid tightened with pulleys. The group conducted a mesh-overlap study by creating a

defect in the abdominal wall, repairing the defect with a mesh, and increasing the pressure of the balloon in steps of 1kPa until failure of the repair site[6]. A limitation of this group's device is the inability to quickly apply a force to the porcine abdominal wall, which is what occurs *in vivo* during a cough.

Dr. Kallinowsky's group constructed a dynamic loading device to simulate the pressures experienced by the abdominal wall during coughing and vomiting on a porcine abdominal wall. In short, this group sought to take a mesh-repaired tissue through a fatigue testing protocol to determine the effectiveness of various repair strategies and products. The dynamic intermittent strain device consisted of an aluminum cylinder equipped with a water-filled plastic bag, which was connected to a pressurized water line. This device was capable of creating pressure spikes of 200mmHg to mimic coughing, and 290 mmHg to mimic vomiting[7]. The group later defined a dimensionless metric known as GRIP to characterize the structural integrity of the repair site. GRIP is a function of the mesh-defect area ratio, the bonding factor, which is dependent on the type and number of fixations, and a successful peritoneal closure. The group found that higher GRIP values led to an increased likelihood to withstand 425 coughing cycles[8]. This group's focus was on the repair's fatigue life, and there has been no work investigating the deformation and mechanical properties of abdominal wall in a physiologically relevant loading environment. Material and interfacial characterization of the abdominal wall under a relevant loading environment is crucial for the development of more effective repair strategies and products, and was the inspiration for this project.

Anatomy of the Abdominal Wall

Four main muscle groups comprise the abdominal wall. These muscle groups are the external oblique, internal oblique, transversus abdominis, and the rectus abdominis[9,10]. A diagram of these muscle groups can be seen in Figure 1 below.

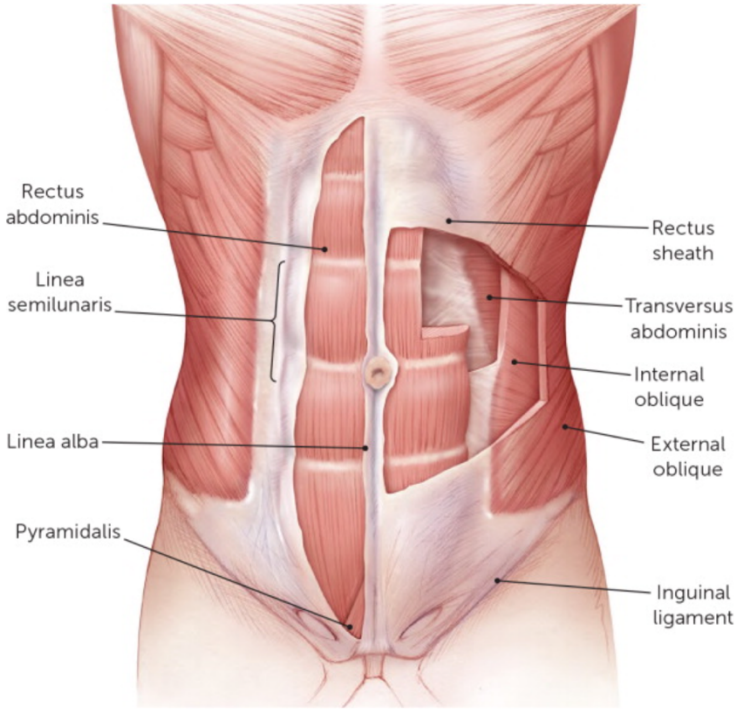

Figure 1: Diagram of anterior abdominal wall[11].

In addition to these muscle groups, it is important to mention the linea alba, the peritoneum, and the rectus sheath.

The external obliques are the most superficial of the anterolateral muscle groups. These muscles contract to twist the trunk to the opposite side of whichever external oblique is contracting. The fibers of the external obliques are directed downward and forward[9,10].

The internal obliques lie posteriorly to the external obliques. Similar to the external obliques, these muscles aid to twist the trunk, but to the same side of whichever internal oblique is contracting. The fibers of the internal obliques are directed upward and forward[9,10].

The transversus abdominis is the deepest of the anterolateral muscle groups, and serves to stabilize the trunk and maintain a proper intra-abdominal pressure. The transversus abdominis is an important muscle for developing a strong and stable abdominal wall[9,10]. The fibers of the transversus abdominis are in the lateromedial direction and this muscle group can be imagined as a belt around the trunk[9].

The rectus abdominis muscles are the most medial of the abdominal muscles. They are strap-like muscles oriented vertically on both sides of the abdominal wall's midline, and are the muscles responsible for the appearance of a "six pack." These muscles are responsible for abdominal flexion resulting in the ability to bend forward. The fibers of the rectus abdominis are oriented vertically[9,10].

The linea alba is a fibrous structure that runs along the midline of the abdominal wall. It is formed by the interlacing aponeuroses of the external oblique, internal oblique, and tranversus abdominis. The linea alba is the attachment point for many muscles and structures, but has minimal structural support posteriorly or anteriorly, which makes it a weak point of the abdominal wall[12]. Because of this, the linea alba is the most common location for ventral hernias.

The peritoneum is a thin membrane that lines the abdominal and pelvic cavities. It is broken into two categories, the parietal peritoneum, which attaches to the posterior side of the abdominal wall, and the visceral peritoneum, which covers the external surfaces of organs within the abdominal cavity[13]. Peritoneal closure is a common maneuver during hernia repairs[14].

The rectus sheath is a fibrous sheath of dense connective tissue that covers the upper three-quarters of the anterior side of the rectus abdominis muscles, and the lower quarter of the anterior side of the rectus abdominis muscles. The primary function of the rectus sheath is to protect the muscles and vessels which it encloses[15].

Development of Project Scope

The goal of the project was to develop a device to apply and measure a representative coughing force applied to a porcine abdominal wall. In addition to loading the tissue, we sought to track three-dimensional abdominal deformation during each loading-unloading cycle. Perhaps the most challenging aspect of the device design was the need for the increase and decrease of pressure to occur very quickly to properly simulate a cough.

The first step of the project was to create a pressure system to apply a coughing force. Next, we sought to measure the force of the cough with time, as to properly determine what point in time the tissue was under maximum load. We then created a 3D strain tracking protocol using the MultiDIC MATLAB toolbox developed by a group at MIT[16]. After determining the accuracy of the strain tracking protocol, we sought to conduct preliminary tests of porcine abdominal wall to prove the effectiveness of the design as a whole.

Chapter 2: Methods and Apparatus

To investigate wound separation after abdominal hernia repair surgeries, a device was constructed to apply a representative coughing force to a porcine abdominal wall. A normal intra-abdominal pressure (IAP) post-surgery is between 3-15 mmHg (0.058-0.29 psi.)[5]. A cough can increase the IAP up to 127 mmHg (2.46 psi.)[3]. This sudden increase in pressure can put significant load on the abdomen and repair site, resulting in wound separation. To better understand the mechanics of the abdominal wall and the mesh-tissue interface, a device was created to expose a porcine abdominal wall to a physiologically relevant loading environment.

Construction of a Dynamic Pressure-Based Loading Device (DPBLD)

The key components of the DPBLD consist of a high-pressure chamber connected to a 17-inch-diameter vinyl balloon via medical tubing with a solenoid valve to control the increase in pressure. The vinyl balloon is housed in an 8x8x8 inch polycarbonate box with an open roof. The outlet of the balloon is connected to a lab vacuum via medical tubing with a solenoid valve to control the decrease in pressure. The open/closed states of the valves are controlled using an Arduino Uno. Further explanation of the components will be addressed in following sections. A schematic of the DPBLD can be seen in Figure 2 below.

Figure 2: Schematic of the DPBLD. Valve 1 opens to increase the pressure to the desired maximum pressure. Valve 1 closes, and simultaneously, valve 2 opens to decrease the pressure back to a normal IAP. Once a normal IAP is reached, valve 2 closes. Valve 1 and valve 2 are both Arduino controlled solenoid valves.

High Pressure Chamber:

The high-pressure chamber was constructed from PVC pipe with 4-inch-diameter and 36-inch-length. The pressure in the high-pressure chamber is 70 psi, which is pressurized using a tank of compressed air with a two-stage regulator. The volume of the high pressure chamber is approximately 450 cubic inches, which is sufficiently large that during the time that valve 1 is open, the pressure in the high-pressure chamber does not greatly decrease.

Polycarbonate Box and Vinyl Balloon:

The high-pressure line and low-pressure line are connected to the inlet and outlet of a vinyl balloon respectively. The vinyl balloon is a spherical shape with a 17 inch diameter and is housed in an 8x8x8 inch polycarbonate box of 0.5-inch wall thickness. The top of the box is open, which is where the abdominal wall is fixed. The top of the box has a radius of curvature of 200 mm to mimic the circumferential curvature of the abdominal wall *in vivo*. As the balloon inflates, it presses against the inside of the box, applying a force against the walls and floor of the

box. Because the abdominal wall is acting as the “lid” to the box, the same force that is acting on the walls and floor of the box also acts on the tissue. An image of the box with the balloon and tissue clamps can be seen in Figure 3 below.

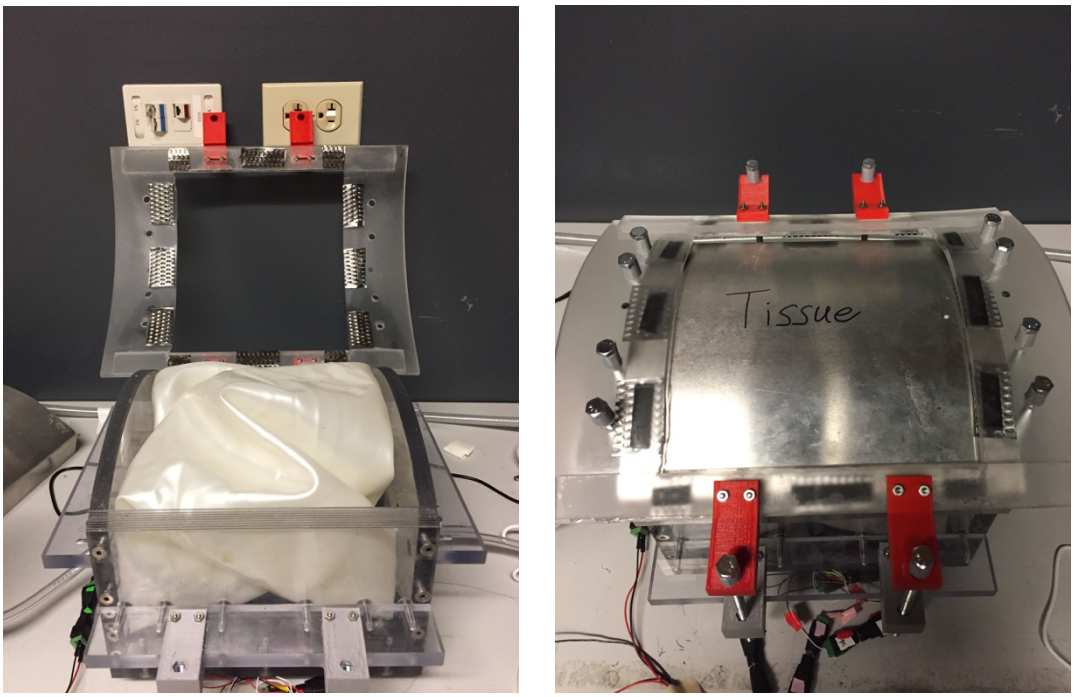

Figure 3: DPBLD polycarbonate box. A vinyl balloon is housed in a polycarbonate box (left). The abdominal wall is placed over the top of the box, and the lid is bolted down to secure the tissue in place. An aluminum plate is fixed in place where the abdominal would be located during testing. The aluminum plate was used as a surrogate abdominal wall during the design and troubleshooting phases of device development (right).

The strips of metal on the underside of the lid of the box are pieces of a cheese grater. The purpose of these metal strips is to bite into the edges of the abdominal wall to prevent it from slipping during loading.

Resting at the bottom of the box is a 1/8 inch thick ABS plate with four load cells in series secured to it. These load cells measure the force that the balloon is exerting on the bottom

of the box. It is assumed that the force exerted on the bottom of the box is also being exerted on the tissue at the top of the box. The load cells are strain gauges that have been calibrated against a pressure gauge to output values that represent the pressure in the balloon rather than the force the balloon is exerting. The load cells were calibrated by first placing the ABS plate in place underneath the balloon. The pressure in the balloon was decreased to zero psi, and the load cells were zeroed. The pressure in the balloon was increased to 3.0 psi determined by a digital pressure gauge with range 0-5 psi. The calibration factor of the load cells was varied until the value output was three orders of magnitude greater than the value displayed on the digital pressure gauge. Although the load cells are technically reading force, they have been calibrated to represent pressure, so from this point forward, measurements taken by the load cells will be referred to as pressure.

Pressure Controller:

The pressure in the balloon is modulated by opening and closing the two solenoid valves. The two valves are controlled via a single Arduino uno, which we will call the valve arduino. The load cells at the bottom of the box send data to a second arduino, which we will call the data arduino, and the data are then read to the serial monitor. The data arduino sends information to the valve arduino to open or close the proper valves when the appropriate pressure values are reached. The pressure controller work flow and user interaction is described below.

In addition to the load cells at the bottom of the box, there is a digital pressure gauge connected to the air line for the user's reference. First, the user presses a button to decrease the pressure in the balloon to 0 psi, and the load cells are zeroed. Then the user increases the pressure in the balloon to between 0.1 and 0.2 psi. Next, the user presses a button to begin data collection, and data is read to the serial monitor. A green LED is turned on while data is being

recorded. When ready, the user presses the "cough button" to begin the coughing simulation. Two seconds after the cough button is pressed, valve 1 (high pressure valve) opens and the pressure begins to increase. Once the pressure exceeds a user defined value, valve 1 closes and valve 2 (low pressure valve) opens, exposing the line to a vacuum. Once the pressure drops below 0.110 psi, valve 2 closes. This method of controlling the valve states means that regardless of the elasticity of the tissue being tested, the pressure will always increase to the desired value.

The data are then copied from the serial monitor into MATLAB for processing. A pressure profile obtained from the aformentioned steps is shown in Figure 4 below. Note that although valve 1 closes when 1.800 psi. is reached, the pressure readings from the load cells continues to rise to ~2.5 psi. While this phenomenon was not thoroughly investigated, one possible explanation is that the balloon is not instantly expanding. Because expansion of the balloon is what is applying the force on the load cells, it is possible that when valve 1 closes, the pressure in the balloon is at a maximum, but because time is needed for the balloon to expand, the maximum force exerted by the balloon occurs slightly later in time.

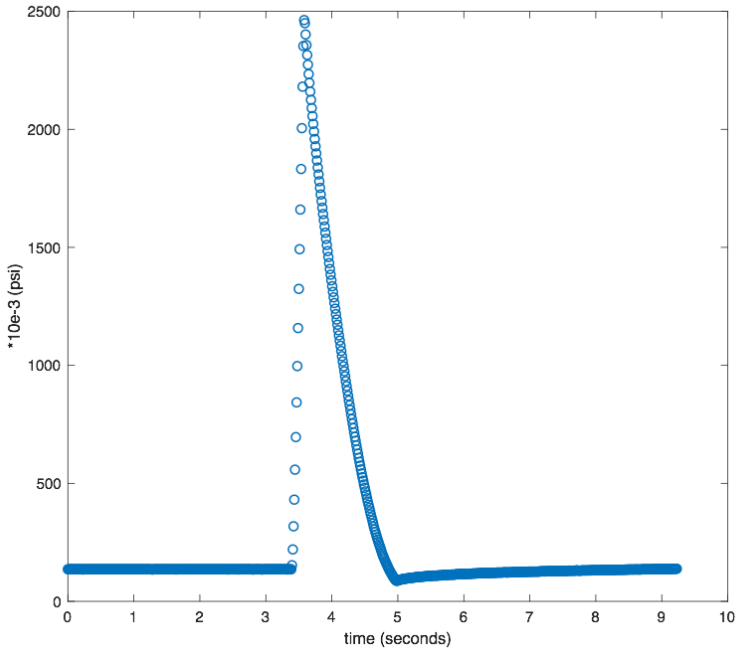

Figure 4: A pressure profile of an applied cough. This data was obtained with an aluminum plate placed over the box (see Figure 3) rather than a tissue sample.

Creation of a Strain Tracking Protocol

In order to properly characterize the deformation of the tissue during an applied cough, it was necessary to track the strain in three dimensions. Using a MultiDIC (Three-dimensional Digital Image Correlation) MATLAB toolbox, developed by a group at MIT, and a Fujifilm Finepix Real 3D W3 camera, we developed a 3D strain tracking protocol. The Fujifilm 3D camera has a focal length of 35mm-105mm. It is equipped with two lenses spaced approximately 60mm apart. The frame rate during video recording is 30 frames per seconds and the frame size is 1280x720 pixels. Utilizing a 3D camera with two lenses rather than a traditional camera with a single lens allows for the triangulation of a three-dimensional coordinate from the set of two-dimensional coordinates captured by each of the two lenses.

In short, the method of strain tracking consists of recording the tissue during the loading-unloading cycle using a stereo camera pair. The tissue is decorated with black Delrin beads, 0.25

inches in diameter as shown in Figure 5 below. The beads are sourced from McMaster Carr, and are originally white, but are spray-painted black. The beads are fixed to the tissue with Loctite 401.

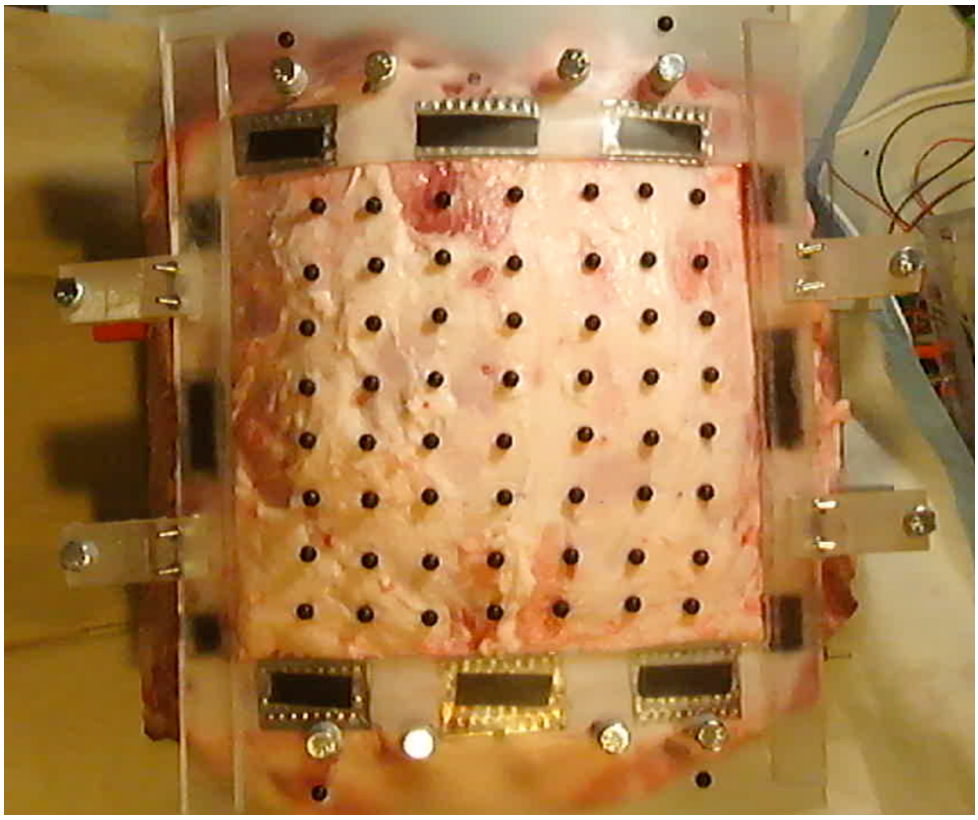

Figure 5: Porcine abdominal wall decorated with black tracking beads. The image above shows a porcine abdominal wall fixed in the DPBLD box. The black tracking beads are used as markers for calculated the three-dimensional deformation of the tissue.

The color/light intensity contrast between the tissue and the beads allows the videos to be color thresholded to exclude all pixels that aren't capturing the beads. A MATLAB code then iterates through each frame of the two stereo videos and finds the location of each bead at each frame in two dimensions. The 3D coordinates of each bead can be determined from the two sets of 2D coordinates and proper calibration settings.

Calibration of the 3D Camera:

The 3D camera, or stereo camera pair, is easily calibrated by taking a stereo picture of a rectangular patterned cylinder. The cylinder used for calibration was 57mm in radius. A pattern of squares was taped to the cylinder. The pattern consists of 6.35mm squares with a center-to-center distance of 12.8mm in both the horizontal and vertical directions. The calibration cylinder can be seen in Figure 6 below.

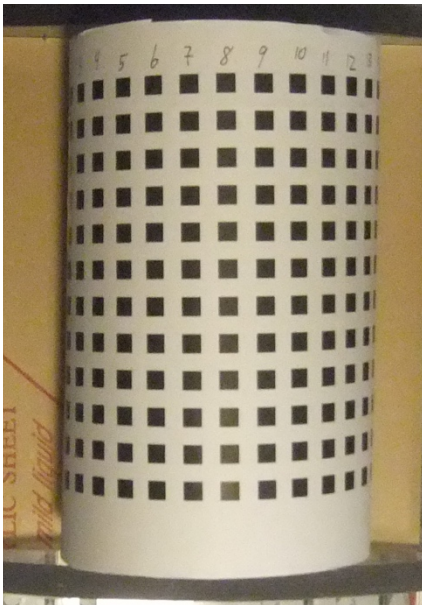

Figure 6: Calibration cylinder. A cylinder of known radius with known locations of each black square is used to calibrate the 3D camera.

The stereo image pair is loaded into a MATLAB code, which is also equipped with the real-world coordinates of each rectangle. The calibration code fits the stereo images to the real-world coordinates and outputs a calibration file and figures describing the accuracy of the calibration. The calibration file is called during the 3D reconstruction of the two sets of 2D coordinates.

Verification of Camera Calibration:

After the camera was calibrated, the performance of the 3D reconstruction was verified using a 3D printed structure with white beads glued at known xyz location. The verification structure can be seen in Figure 7 below.

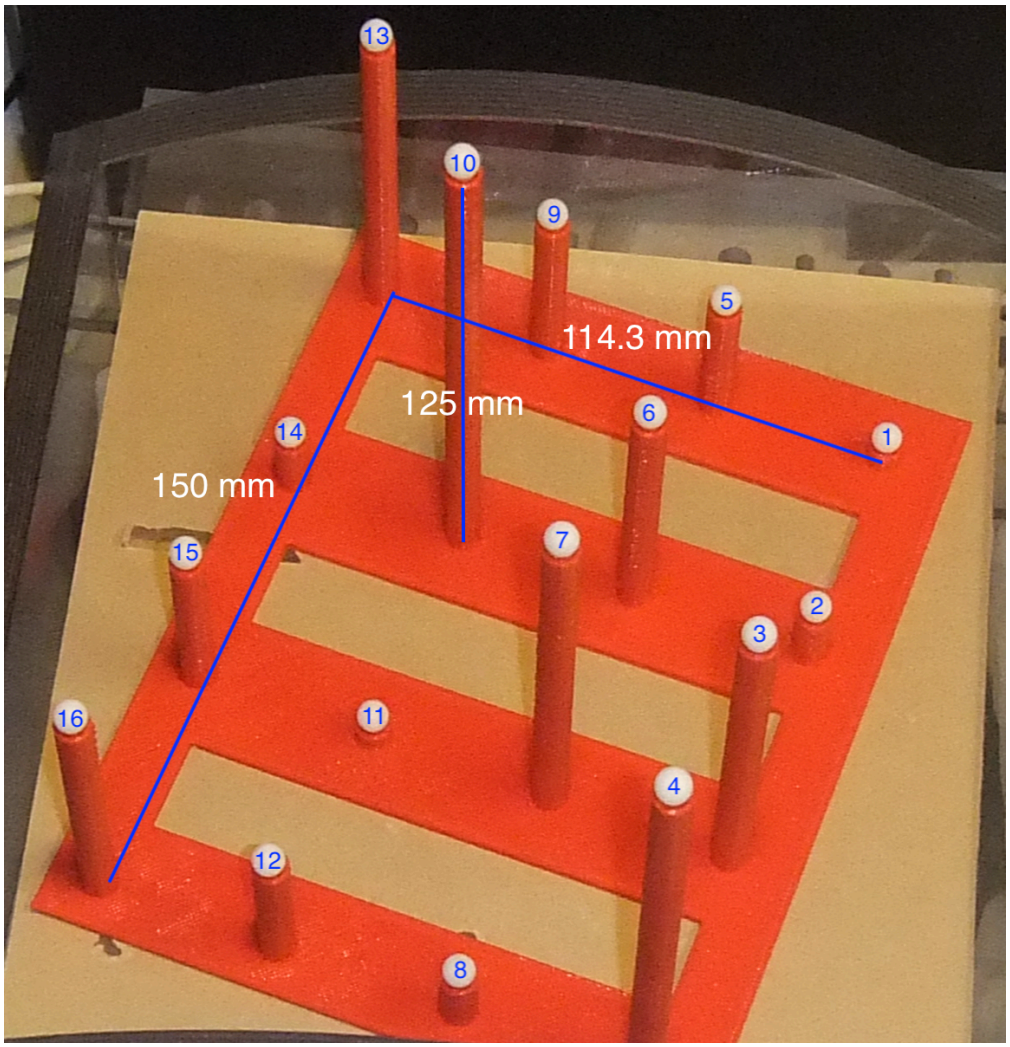

Figure 7: 3D camera verification structure. White beads are glued to the top of each post of this 3D printed structure. The location of each bead relative to bead 1 is known.

This verification structure was 3D printed with PLA using a MakerBot Replicator 2 desktop 3D-printer. When viewed in plane, the posts are arranged in a grid, with the distance

from the bottom of post 1 to the bottom of post 2 being 50mm apart and the bottom of post 1 to the bottom of post 5 being 38.1 mm apart. The change in height between bead 1 and bead 10, the lowest and highest beads respectively, is 120mm. The beads are made of Delrin, are 0.25 inches in diameter, and are fixed to the top of each post with Loctite 401. The verification structure was designed to be placed in the box of the DPBLD with the lowest and highest beads located below and above the bounds created by the lowest and highest locations of the abdominal wall during loading.

The known 3D coordinates of each bead were used to calculate the distance from each bead to bead 1. Similarly, the 3D coordinates output by MATLAB were used to determine the distance from each point to bead 1. These distances were then compared to determine the level of accuracy. This method of verification was chosen because the reference frame of the reconstructed 3D coordinates is not perfectly aligned with the known coordinate reference frame. The necessary coordinate transformation is difficult to determine because the accuracy of any individual reconstructed point is not known, and thus makes choosing the reference points for a transformation difficult. The accuracy of the calibration will be revisited in Chapter 3.

Abdominal Wall Preparation and Testing:

After the completion of the previously mentioned tasks, a porcine abdominal wall was subjected to mechanical testing and strain tracking. The porcine abdominal wall was allowed to thaw from frozen overnight. The skin and subcutaneous fat were removed from the sample. Using a biopsy punch, several holes (eight or more depending on the size of the tissue), were created around the perimeter of the sample. An aluminum frame with posts was used to pull the tissue taut and provide easy transportation to the DPBLD. The location of the posts of the frame were adjusted according to the location of the biopsy punched holes. The tissue was pulled taut

and the posts were inserted into the holes to hold the tissue in place. Attention was paid to have the linea alba at the midline of the aluminum frame. Black plastic beads (tracking beads), 0.25 inches in diameter, were attached using Loctite 401 to the anterior side of the abdominal wall. The workflow of the steps above can be seen in Figure 8 below.

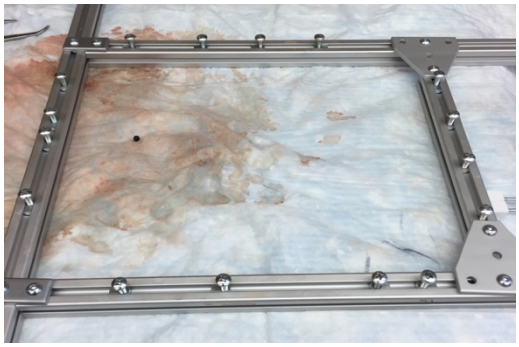

1: The aluminum frame with adjustable posts aids in pulling the tissue taut

2: The skin and subcutaneous fat are removed from the tissue sample

3: The tissue sample is mounted on the posts of the aluminum frame via holes created with a biopsy punch

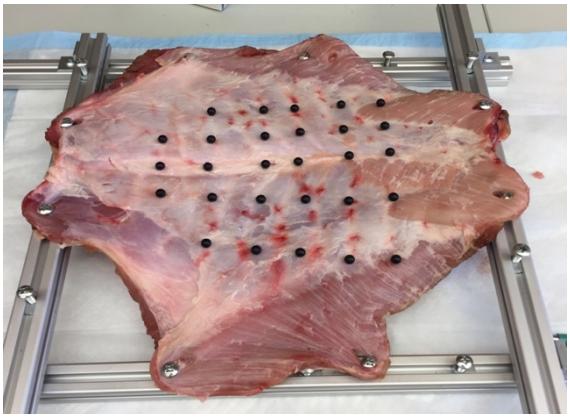

4: The tissue sample is decorated with black tracking beads

Figure 8: Abdominal wall preparation. The images above show the steps taken to prepare the abdominal wall for testing.

The tissue, with the aluminum frame, is then transferred to the DPBLD. The tissue is placed over the open box such that the linea alba is parallel with the axis of curvature of the box, and the aluminum frame is resting on the outside of the box. The lid of the box is placed over the tissue and bolted in place. A hand drill with a clutch is used to tighten each of the 12 bolts,

and the clutch ensures each bolt is tightened the same amount. As this point, the tissue is securely fixed to the box, and the aluminum frame is removed. An image of the tissue secured to the box can be seen in Figure 9 below.

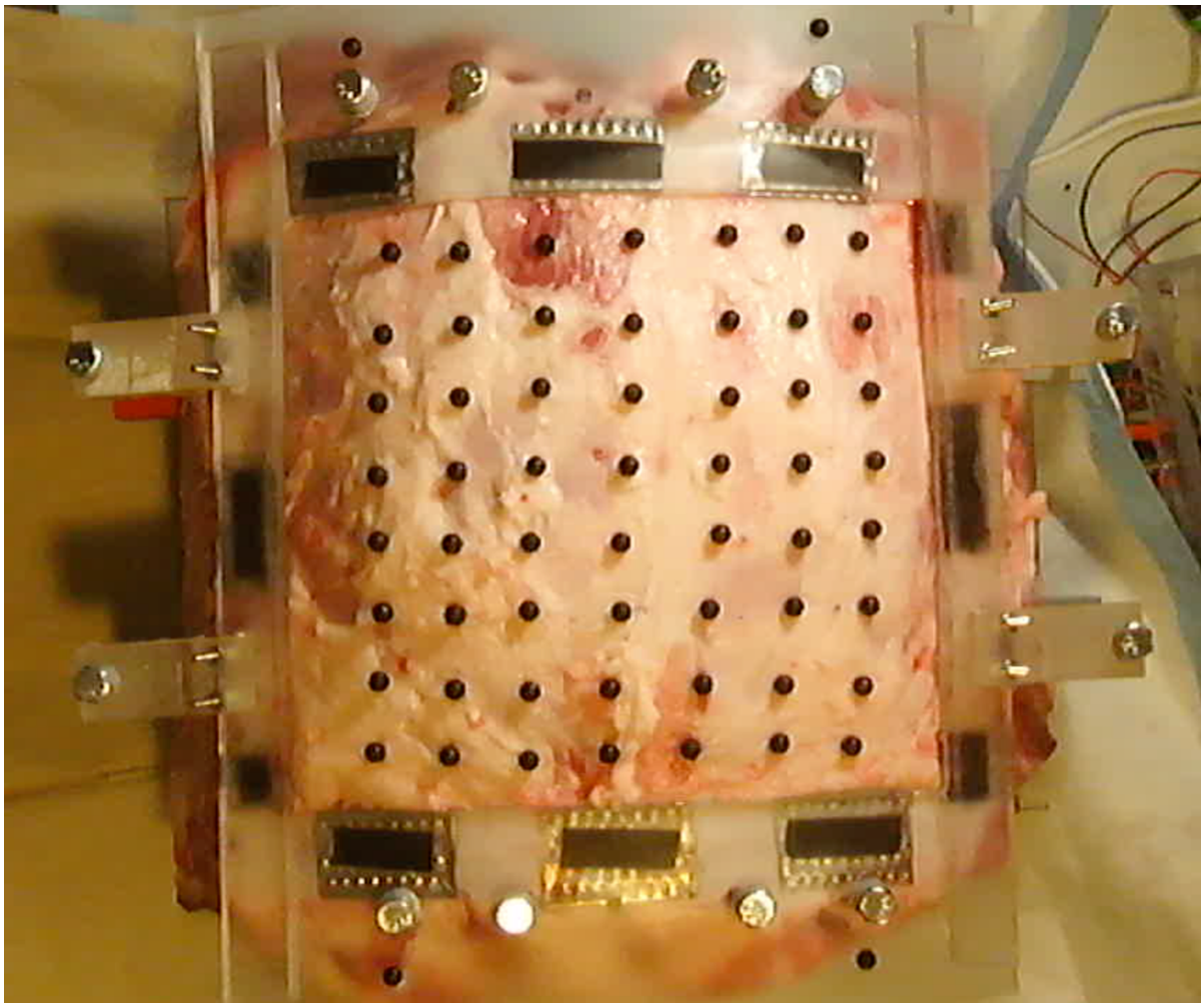

Figure 9: Porcine abdominal wall secured to DPBLD box. The lid of the box is tightened down by the 12 bolts. The strips of cheese grater bite into the sample to prevent slipping.

The abdominal wall was subjected to 12 total coughing cycles of four different intensities. As mentioned, the high-pressure valve closes once a desired pressure reading is

reached. The four intensities were varied by closing the high-pressure valve and opening the low-pressure valve at pressures of 1.4psi, 1.8psi, 2.2psi, and 2.6psi.

After testing, 3D videos were cropped so that the video begins at the first frame the green LED is on and ends at the first frame the LED turns off. This step is necessary to bring the video data and pressure data into the same temporal reference frame. The 3D video file was then split into two stereo videos. The 3D coordinates of each bead at each frame were determined via the MATLAB code previously described.

Chapter 3: Results and Discussion

Verification of Strain Tracking Protocol

As mentioned in Chapter 2, the 3D camera was calibrated using a cylinder of known radius decorated with a rectangular pattern of squares with known locations. The camera was calibrated using an image of this cylinder, and the calibration parameters were calculated based on 120 points on the cylinder. An image of the cylinder's reconstructed points, along with the reconstruction error statistics over all points can be seen in Figure 10 and Figure 11 respectively.

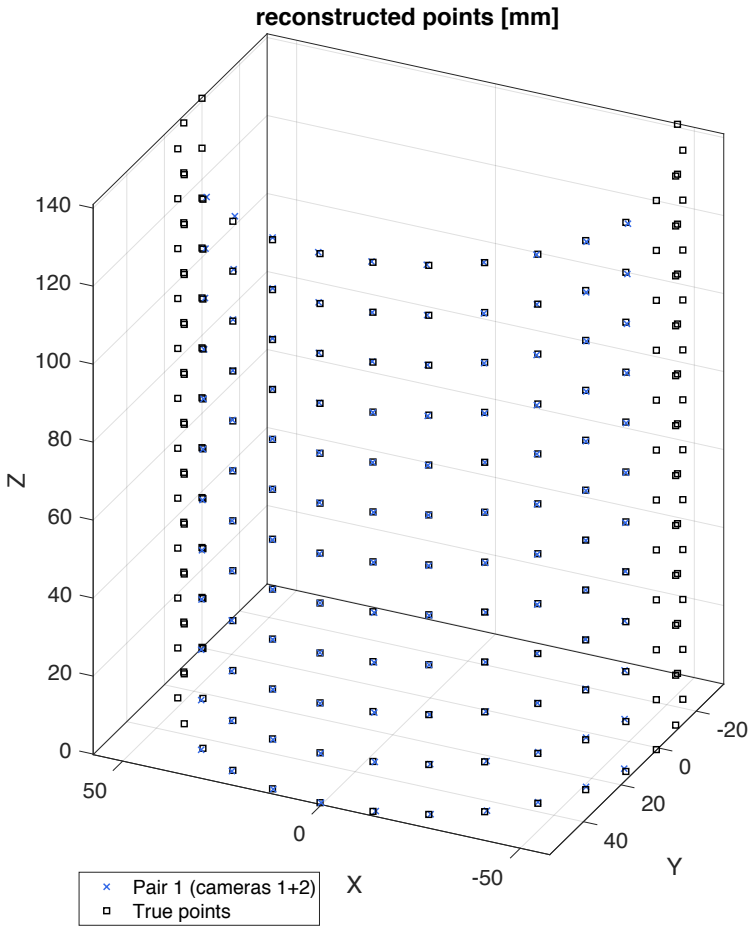

Figure 10: 3D coordinate reconstruction of calibration cylinder.

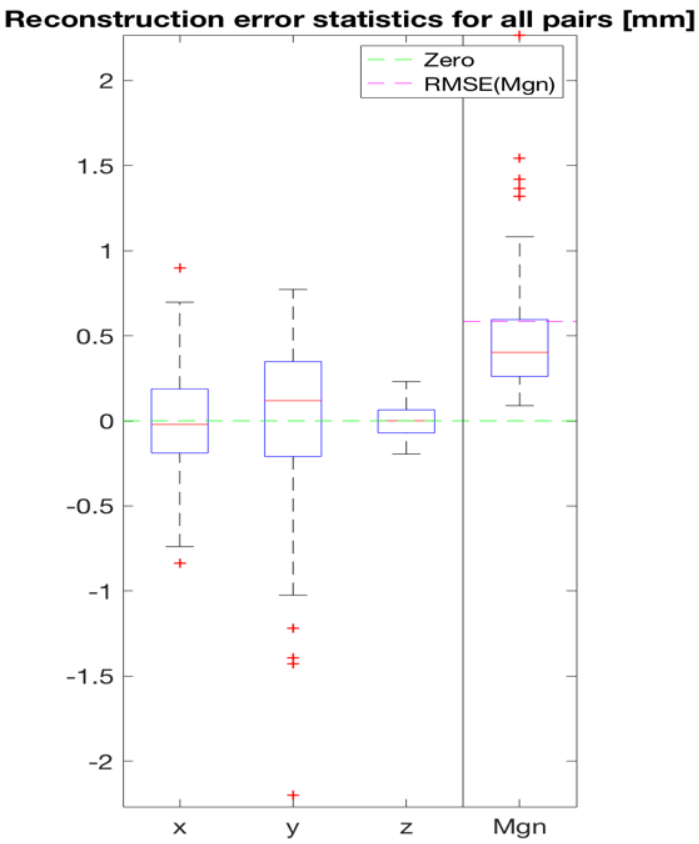

Figure 11: Reconstruction error statistics of calibration cylinder coordinates.

By visual inspection, it is clear that the reconstructed point locations are well aligned with the true point locations. The reconstruction errors in the x, y, and z directions are 0.0215mm, 0.1186mm, and 0.0006mm respectively. When considering these errors, it is important to note how the directions are related to the stereo camera's positioning. The direction created by drawing a line from one camera lens to the other camera lens corresponds to the x direction. The y direction is the depth towards or away from the camera, and corresponds to a line going from the midpoint of the two camera lenses to the circumferential surface of the cylinder. The z direction corresponds to the direction of a line going from the midpoint of the two camera lenses moving perpendicular to the line between the camera lenses and parallel to the

centerline of the cylinder. It is not surprising that the error in the z-direction is smallest because the translation from one lens to the other lens takes place only in the x-direction. A diagram describing these directions can be seen in Figure 12 below.

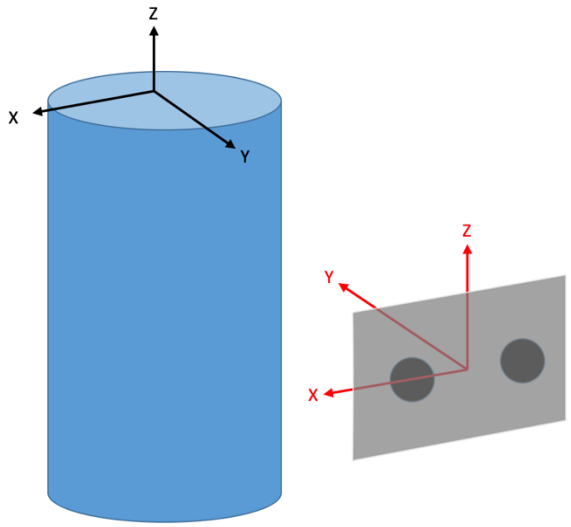

Figure 12: Reference frame of camera relative to cylinder. The line created between one lens and the other lens has components only in the x-direction. The camera reference frame is mirrored about the x-z plane of the cylinder's reference frame. The y coordinate values output by the MATLAB code decrease as a point moves closer to the camera.

After calibrating the camera and creating a calibration file, the effectiveness of the 3D reconstruction was tested using the structure with known bead locations shown in Figure 7 above. As previously mentioned, the distance from bead 1 to all other beads was calculated based on the known 3D coordinates. Table 1 below shows the accuracy of these distance calculations.

Table 1: Verification of Reconstructed Point to Point Distances

Distance from Point 1 to Point…	Known Distance (mm)	Reconstructed Distance (mm)	Error (mm)		Percent Error (%)	
2	50.99	51.38	0.39		0.77	
3	128.06	128.78	0.72		0.56	
4	186.01	185.52	-0.49		0.26	
5	48.49	48.87	0.38		0.78	
6	86.90	86.88	-0.02		0.02	
7	139.83	139.74	-0.09		0.06	
8	155.09	155.26	0.17		0.11	
9	86.06	86.23	0.17		0.19	
10	150.69	150.02	-0.67		0.44	
11	125.72	125.36	-0.37		0.29	
12	170.90	170.25	-0.65		0.38	
13	139.52	138.31	-1.20		0.86	
14	125.16	124.17	-0.99		0.79	
15	157.05	155.47	-1.58		1.01	
16	197.90	195.76	-2.14		1.08	
			Mean -0.42	**Standard Deviation 0.77**	**Mean 0.51**	**Standard Deviation 0.34**

As you can see, the average error in distance from bead 1 to each of the 15 other beads is -0.42mm, with a standard deviation of 0.77mm.

Tissue Loading Results

The tissue went through 12 total loading-unloading cycles. For cycles 1-3, the high-pressure valve closed at 1.4 psi. For cycles 4-6, the high-pressure valve closed at 1.8 psi. For

cycles 7-9, the high-pressure valve closed at 2.2 psi. For cycles 10-12, the high-pressure valve closed at 2.6 psi.

The 3D coordinates of each tracking bead were determined at each frame of the video. Using cubic interpolation about the tracking markers, a mesh was created for the normal IAP and the frame at which the tissue was exposed to the maximum pressure. Figure 13 below contains an example of these two mesh reconstructions as well as a contour map of the y-location as a function of the x and z locations. The mesh reconstructions and contour maps of all trials can be found in Appendix A-D.

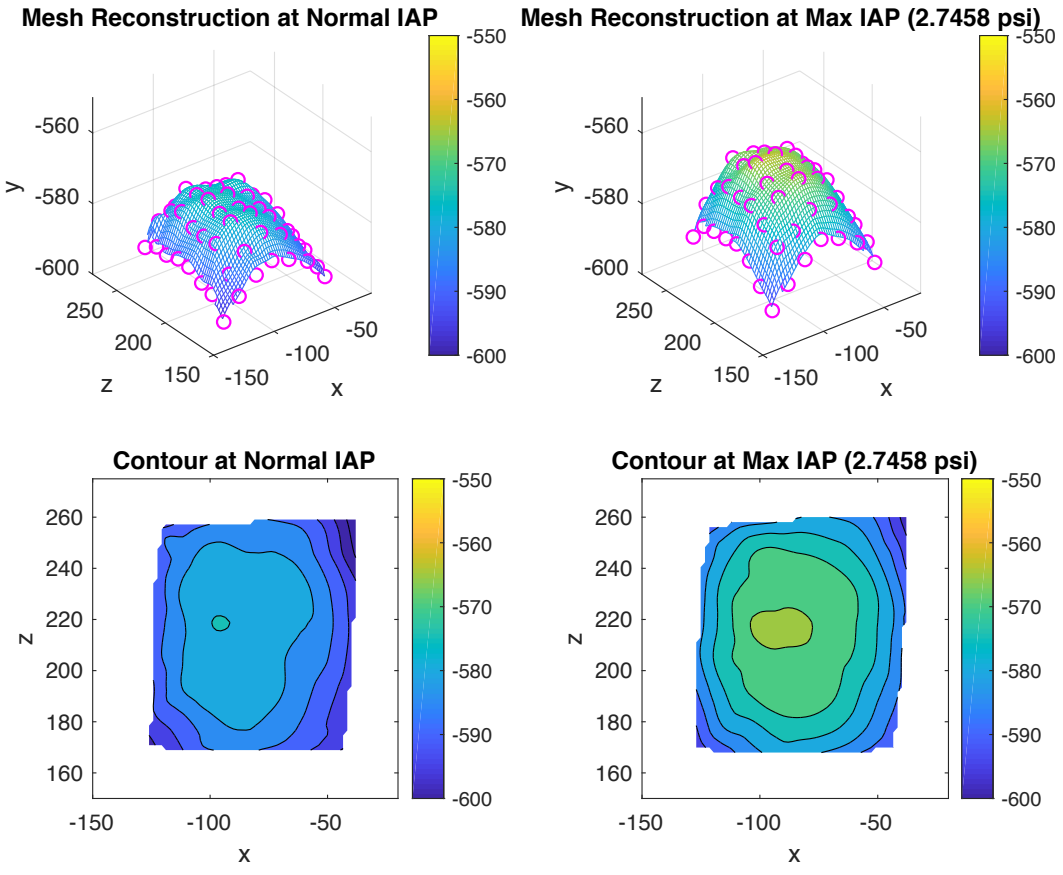

Figure 13: Mesh reconstructions and contour plots of the abdominal wall at normal IAP and maximum IAP.

Similarly, the total displacement between each marker's normal IAP location and each marker's maximum IAP location was determined. A mesh reconstruction and contour map of this total displacement as a function of the x and z coordinates was then determined. This displacement can be seen in Figure 14 below. The mesh reconstructions and contour maps of displacement of all trials can be found in Appendix A-D.

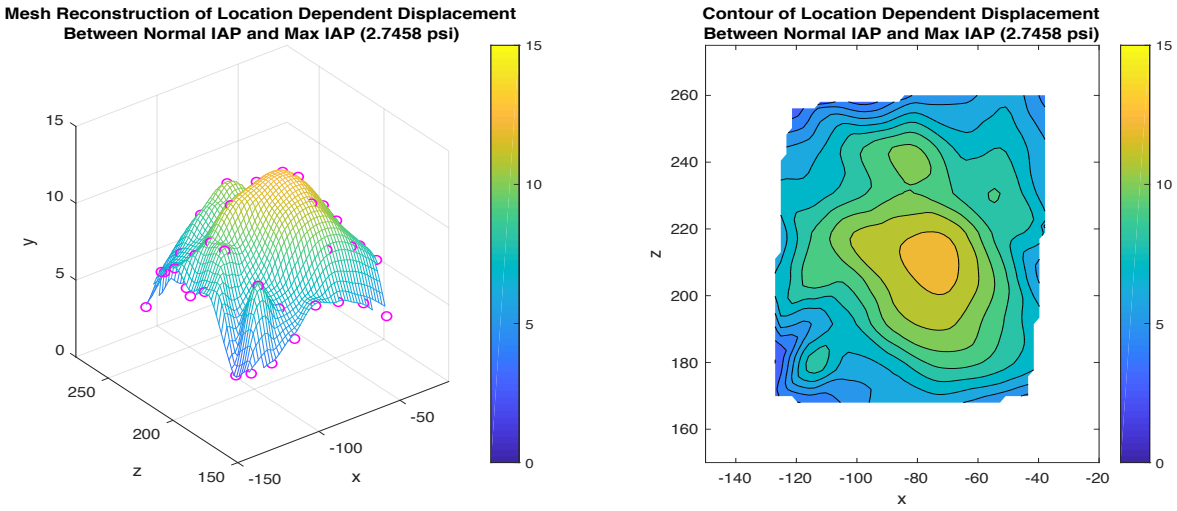

Figure 14: Mesh reconstruction and contour plot of abdominal displacement between normal IAP and maximum IAP.

Lastly, Table 2 below displays the key parameters that describe the applied loads and the way in which the tissue responded. This table includes the programmed values at which the high-pressure valve closes, the maximum pressure reached, the duration of the cough, and the maximum height (y-direction) reached by the tissue during loading. The duration of the cough was defined as the time is takes to go from 0.380 psi on the ascending side of the cough back to 0.380 psi on the descending side of the cough. The value of 0.380 psi was chosen based on the condition known as abdominal compartment syndrome. Abdominal compartment syndrome is defined as having an IAP greater than 20mmHg (0.3867psi)[17]. Between the IAP associated with abdominal compartment syndrome, and a post-operative IAP of 3-15 mmHg (0.058-0.29 psi)

being considered normal[5], it was decided that 0.380 psi was an appropriate value to determine the start and end of the cough. The maximum height reached by the tissue during loading was determined by first creating a 20x20 grid in the x and z directions based off of the x and z locations of each marker. The height (y-direction) of each marker was then used to fit a cubically interpolated data set dependent on the 20x20 grid found from the x and z locations to create a mesh. The six highest points of this mesh were then determined, and the two highest points were discarded to reduce the effect of outliers. An average was taken over the four remaining values. The average y-coordinate of three stationary tracking beads placed on the DPBLD box itself was then subtracted from the average maximum height value.

Table 2: Key Parameters of Applied Coughing Cycles

High Pressure Valve Close Value (psi)	Max Pressure Value (psi)		Cough Duration (ms)		Maximum Height (mm)	
1.4	1.852	**Average 1.954**	1079	**Average 1098**	29.51	**Average 29.30**
1.4	2.022		1126		28.73	
1.4	1.989		1089		29.64	
1.8	2.326	**Average 2.391**	1273	**Average 1302**	31.09	**Average 32.34**
1.8	2.438		1322		31.45	
1.8	2.410		1310		34.46	
2.2	2.749	**Average 2.779**	1497	**Average 1514**	34.66	**Average 35.39**
2.2	2.817		1548		35.70	
2.2	2.772		1496		35.80	
2.6	3.192	**Average 3.171**	1725	**Average 1711**	37.31	**Average 38.90**
2.6	3.135		1687		37.62	
2.6	3.185		1722		41.77	

The data presented in Table 2 above shows the device's ability to apply coughing forces of varying severities by altering the value at which the high pressure valve closes after the balloon begins inflating. In addition, it is shown that the peak pressure of the applied cough has a direct impact on the response of the tissue. For example, when the cough with a peak pressure

of 1.954 psi is applied, the abdominal wall's height displacement is 29.30 mm. When the cough with a peak pressure of 3.171 psi is applied, the abdominal wall's height displacement is 38.90 mm. These results are expected because like all materials, increasing the force results in a greater displacement.

Chapter 4: Recommendations and Conclusions

The purpose of this project was to design a device to apply and measure a representative coughing force applied to a porcine abdominal wall and track the tissue displacement in three dimensions. The dynamic pressure-based loading device (DPBLD) was constructed and equipped with a user-friendly Arduino-based controller. In addition, a 3D strain tracking protocol was developed using the MultiDIC MATLAB toolbox. I have demonstrated the ability of the DPBLD to produce repeatable coughing forces to the abdominal wall and have shown the effectiveness of the strain tracking protocol.

Due to time constraints and the impact of COVID-19 on the capacity to conduct on-site work, there are four modifications that were not possible to explore but should be given future attention to more effectively utilize the tools and protocols that have been developed.

First, the single 3D camera should be replaced by a set of three stereo cameras. These cameras are to be positioned in a triangular pattern and should be farther apart than the two lenses of the 3D camera. Moving the cameras farther apart will result in greater differences in the line of sight of each camera. A more exaggerated line of sight change will allow for more accurate 3D reconstructions. Furthermore, it is expected that utilizing three cameras in a triangular arrangement will result in less calibration error in the x-direction, which in turn, will increase the accuracy and precision of the y-direction. Referring back to the reconstruction errors described in Chapter 3, the x-direction showed significantly more error than the z-direction because the translation from one camera lens to the other lens was a translation that occurred only in the x-direction. By utilizing three cameras with translation vectors in both the x-direction and z-direction, it is expected that the error in the x-direction will decrease. Because

the y-direction is reconstructed from the x- and z-directions, a decreased x-direction error will also decrease the y-direction error.

Second, the location and intensity of the light source during video recording is critical to the ability to accurately and reliably threshold the tracking beads. It is recommended that four light sources be utilized. The line of sight for each light source should bisect each of the four corners of the DPBLD. Each light source should be raised approximately 60 degrees above the plane created by the four corners of the DPBLD. If possible, the intensity of light should be bright enough to saturate all pixels that do not contain the tracking beads. Utilizing four light sources in the positions described will eliminate shadows caused by the tracking beads and will result in sharper contrast between each bead and the surrounding tissue, making thresholding easier and more reliable.

Third, to make testing easier, reduce the post-processing time, and more accurately align the videos with the pressure data in time, an external switch should be utilized to start and stop the video recordings. The external switch can be wired to the data collection button on the DPBLD controller. If done successfully, this will begin the recording at the same point in time that data collection begins and end the recording at the exact time that data collection ends. Compared to cropping the video based on the visual cue of a light turning on or off, this modification will save post-processing time, but more importantly, will align the video with the pressure data with much more accuracy and precision.

Finally, the effect of friction between the balloon and the posterior side of the abdominal wall should be investigated. If the posterior side of the abdominal wall is not able to slide over the surface of the balloon during loading, there is the possibility that the tissue is experiencing shear due to the high friction between the balloon and the posterior side of the abdominal wall.

While the relative magnitude of shear experienced is unknown and may not be of importance, applying a thin layer of lubricant, such as petroleum jelly, could greatly decrease the effects of friction.

While only one abdominal wall was successfully tested, the progress made on this project will pave the way for future investigations of ventral hernia repair strategies and products. We now have the ability to expose a porcine abdominal wall to a physiologically relevant loading environment and track three-dimensional abdominal deformation during the applied cough. The DPBLD and deformation tracking protocol can be utilized to investigate the effectiveness of various repair strategies and products on returning native tissue function. There is now the opportunity to design and conduct experiments that were previously not possible.

References

1. Laparoscopic Ventral Hernia Repair Information from SAGES. (2015, March 1). Retrieved from https://www.sages.org/publications/patient-information/patient-information-for-laparoscopic-ventral-hernia-repair-from-sages/
2. Deeken, C. R., & Lake, S. P. (2017). Mechanical properties of the abdominal wall and biomaterials utilized for hernia repair. *Journal of the Mechanical Behavior of Biomedical Materials*, *74*, 411–427. doi: 10.1016/j.jmbbm.2017.05.008
3. Cobb, W. S., Burns, J. M., Kercher, K. W., Matthews, B. D., Norton, H. J., & Heniford, B. T. (2005). Normal Intraabdominal Pressure in Healthy Adults. *Journal of Surgical Research*, *129*(2), 231–235. doi: 10.1016/j.jss.2005.06.015
4. Johns Hopkins Medicine. (n.d.). Ventral (Abdominal) Hernia. Retrieved from https://www.hopkinsmedicine.org/health/conditions-and-diseases/hernias/ventral-abdominal-hernia
5. Rao, P., Chaudhry, R., & Kumar, S. (2006). Abdominal Compartment Pressure Monitoring – A Simple Technique. *Medical Journal Armed Forces India*, *62*(3), 269–270. doi: 10.1016/s0377-1237(06)80017-1
6. Lyons, M., Mohan, H., Winter, D. C., & Simms, C. K. (2015). Biomechanical abdominal wall model applied to hernia repair. *British Journal of Surgery*, *102*(2). doi: 10.1002/bjs.9687
7. Siassi, M., Mahn, A., Baumann, E., Vollmer, M., Huber, G., Morlock, M., & Kallinowski, F. (2014). Development of a dynamic model for ventral hernia mesh repair. *Langenbecks Archives of Surgery*, *399*(7), 857–862. doi: 10.1007/s00423-014-1239-x
8. Kallinowski, F., Harder, F., Gutjahr, D., Raschidi, R., Silva, T. G., Vollmer, M., & Nessel, R. (2018). Assessing the GRIP of Ventral Hernia Repair: How to Securely Fasten DIS Classified Meshes. *Frontiers in Surgery*, *4*. doi: 10.3389/fsurg.2017.00078
9. The Editors of Encyclopaedia Britannica. (2017, September 17). Abdominal muscle. Retrieved from https://www.britannica.com/science/abdominal-muscle
10. Department of Health & Human Services. (2015, June 30). Abdominal muscles. Retrieved from https://www.betterhealth.vic.gov.au/health/conditionsandtreatments/abdominal-muscles
11. Shian, B., & Larson, S. T. (2018, October 1). Abdominal Wall Pain: Clinical Evaluation, Differential Diagnosis, and Treatment. Retrieved from https://www.aafp.org/afp/2018/1001/p429.html
12. Zaikauskaite, E. (2020, March 25). Linea alba. Retrieved from https://www.kenhub.com/en/library/anatomy/linea-alba
13. Colorado State University. (n.d.). Peritoneum, Mesentery, and Omentum. Retrieved from http://www.vivo.colostate.edu/hbooks/pathphys/digestion/basics/peritoneum.html
14. Kane, E. D., Leduc, M., Schlosser, K., Parentela, N., Wilson, D., & Romanelli, J. R. (2017). Comparison of peritoneal closure versus non-closure in laparoscopic trans-abdominal preperitoneal inguinal hernia repair with coated mesh. *Surgical Endoscopy*, *32*(2), 627–637. doi: 10.1007/s00464-017-5712-9

15. Vasković, J. (2020, March 23). Rectus sheath. Retrieved from https://www.kenhub.com/en/library/anatomy/rectus-sheath
16. Solav, D., Moerman, K. M., Jaeger, A. M., Genovese, K., & Herr, H. M. (2018). MultiDIC: An Open-Source Toolbox for Multi-View 3D Digital Image Correlation. *IEEE Access*, *6*, 30520–30535. doi: 10.1109/access.2018.2843725
17. Al-Abassi, A. A., Saadi, A. S. A., & Ahmed, F. (2018). Is intra-bladder pressure measurement a reliable indicator for raised intra-abdominal pressure? A prospective comparative study. *BMC Anesthesiology*, *18*(1). doi: 10.1186/s12871-018-0539-z

Appendix A: Mesh Reconstructions of Trials 1-3 (High Pressure Valve Closes at 1.4 psi)

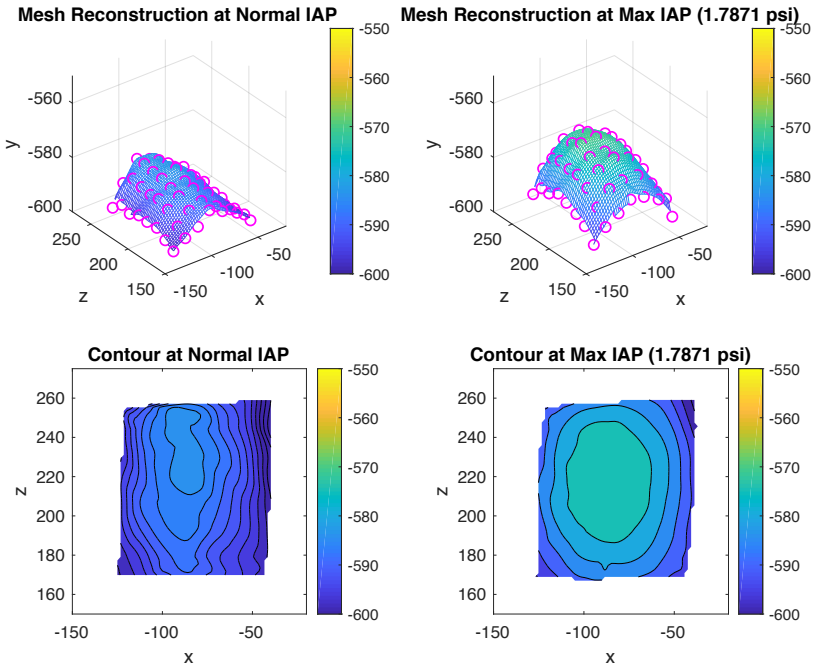

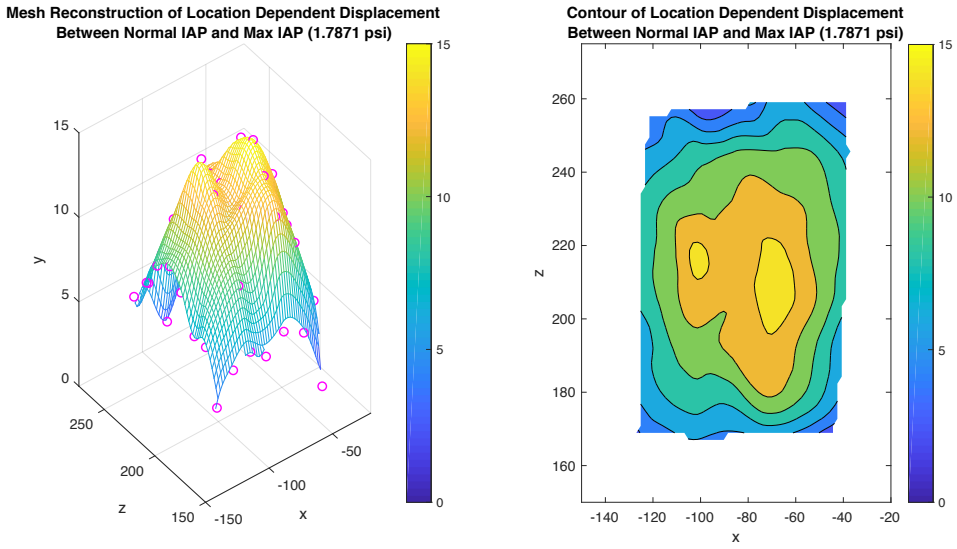

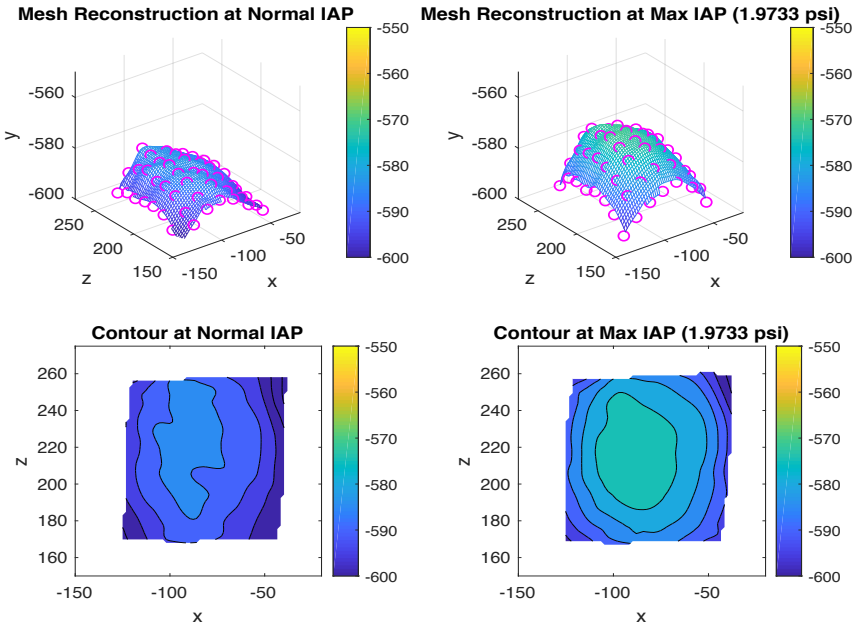
Mesh Reconstruction at Normal IAP
Mesh Reconstruction at Max IAP (1.9733 psi)
Contour at Normal IAP
Contour at Max IAP (1.9733 psi)
x
y
z

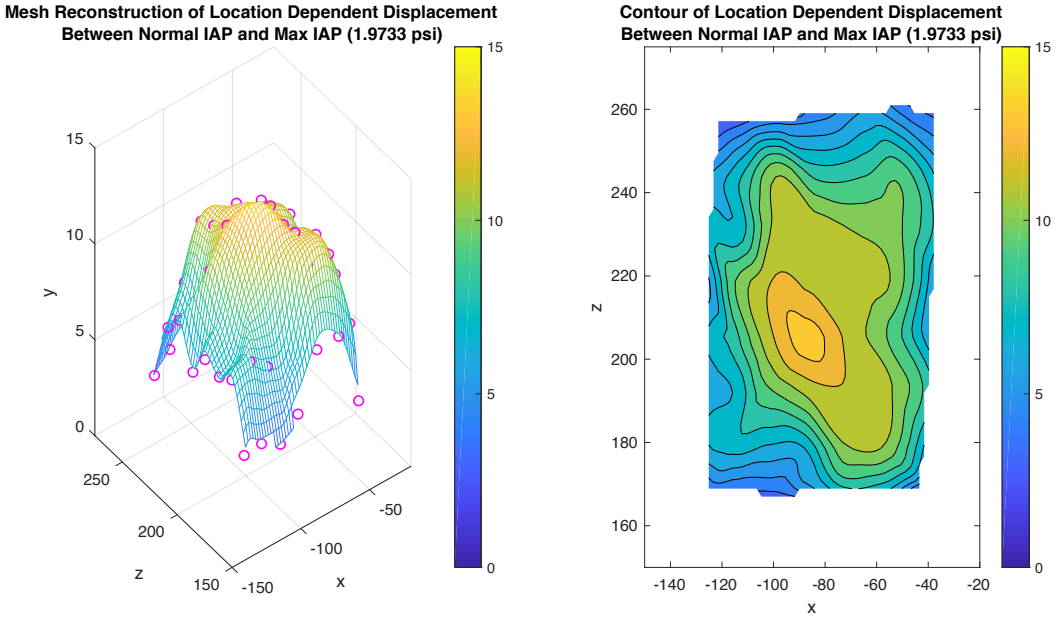
Mesh Reconstruction of Location Dependent Displacement
Between Normal IAP and Max IAP (1.9733 psi)
Contour of Location Dependent Displacement
Between Normal IAP and Max IAP (1.9733 psi)
x
y
z

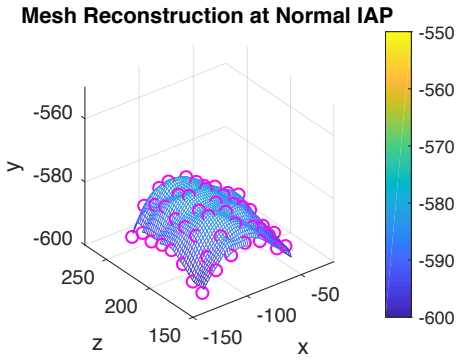
Mesh Reconstruction at Normal IAP
-560
-580
-600
y
250
200
150
z
-150
-100
-50
x
-550
-560
-570
-580
-590
-600

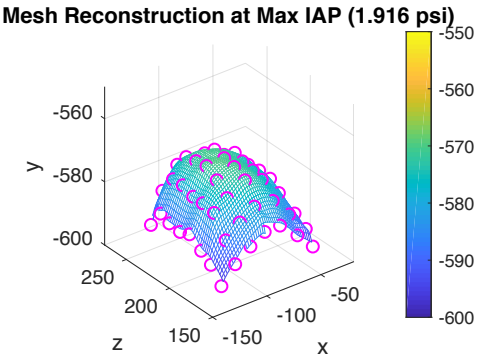
Mesh Reconstruction at Max IAP (1.916 psi)
-560
-580
-600
y
250
200
150
z
-150
-100
-50
x
-550
-560
-570
-580
-590
-600

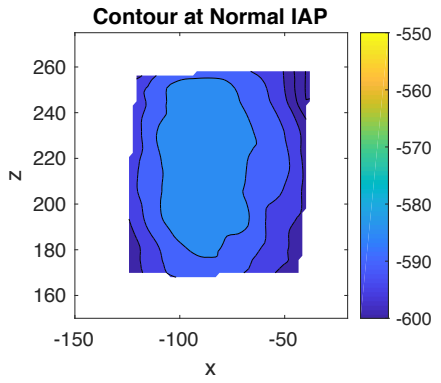
Contour at Normal IAP
260
240
220
200
180
160
z
-150
-100
-50
x
-550
-560
-570
-580
-590
-600

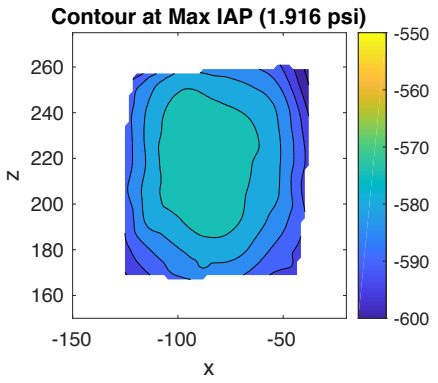
Contour at Max IAP (1.916 psi)
260
240
220
200
180
160
z
-150
-100
-50
x
-550
-560
-570
-580
-590
-600

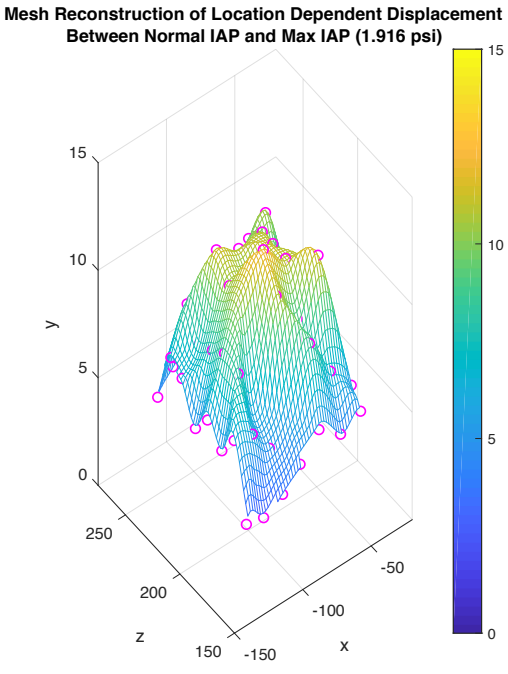
Mesh Reconstruction of Location Dependent Displacement
Between Normal IAP and Max IAP (1.916 psi)
15
10
5
0
y
250
200
150
z
-150
-100
-50
x
15
10
5
0

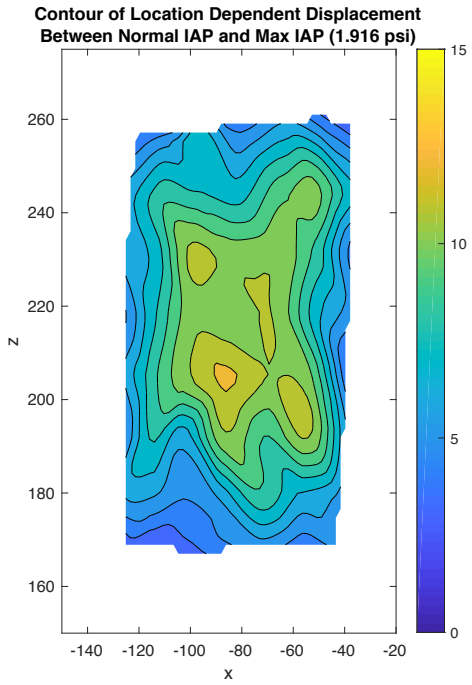
Contour of Location Dependent Displacement
Between Normal IAP and Max IAP (1.916 psi)
260
240
220
200
180
160
z
-140
-120
-100
-80
-60
-40
-20
x
15
10
5
0

Appendix B: Mesh Reconstructions of Trials 4-6 (High Pressure Valve Closes at 1.8 psi)

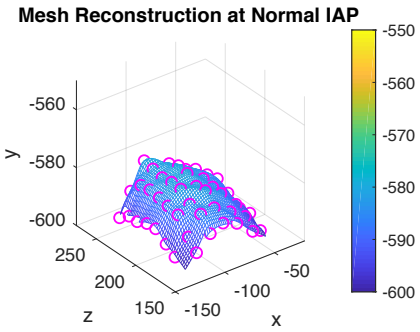

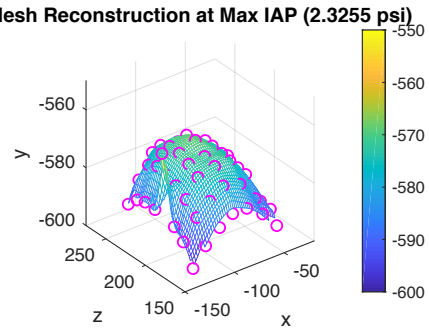

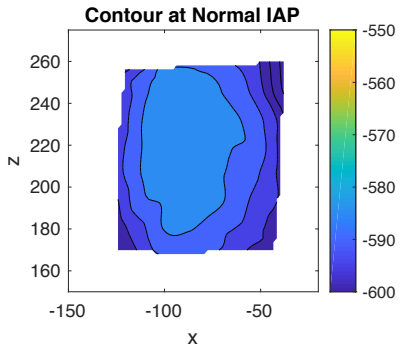

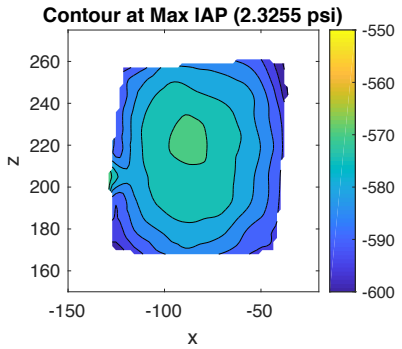

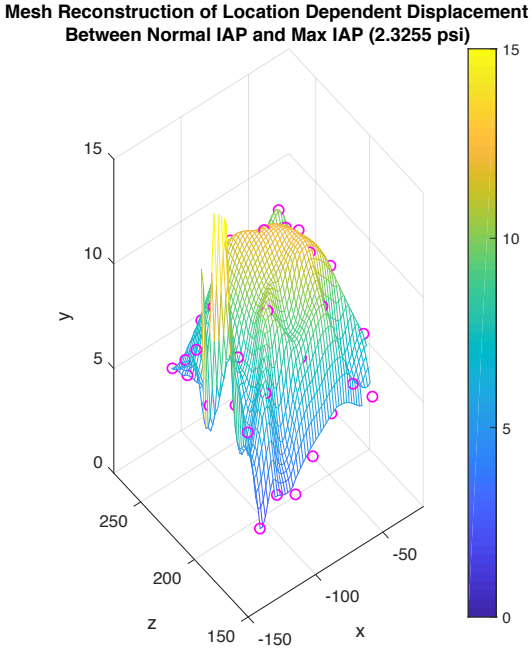

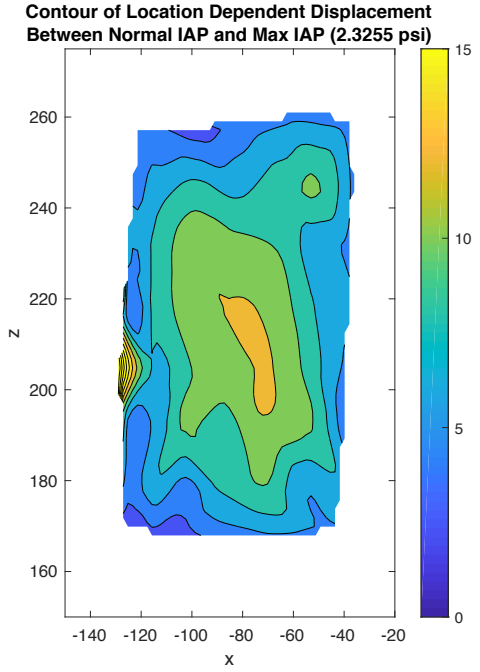

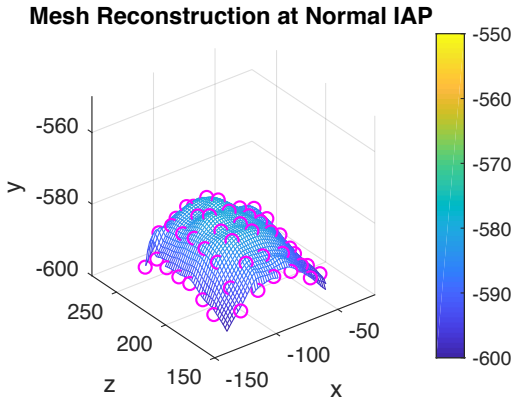
Mesh Reconstruction at Normal IAP
y
-560
-580
-600
250
200
150
z
-150
-100
-50
x
-550
-560
-570
-580
-590
-600

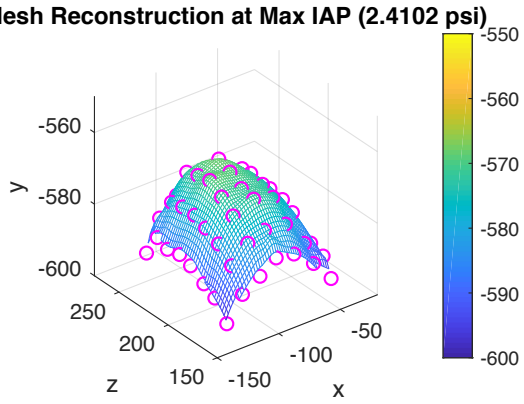
Mesh Reconstruction at Max IAP (2.4102 psi)
y
-560
-580
-600
250
200
150
z
-150
-100
-50
x
-550
-560
-570
-580
-590
-600

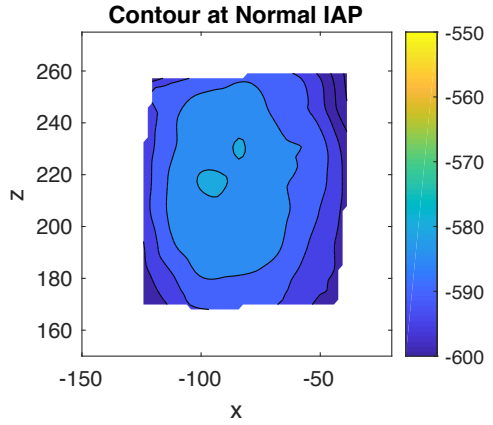
Contour at Normal IAP
z
260
240
220
200
180
160
-150
-100
-50
x
-550
-560
-570
-580
-590
-600

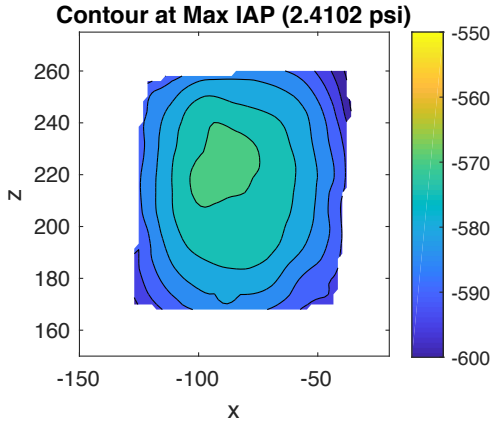
Contour at Max IAP (2.4102 psi)
z
260
240
220
200
180
160
-150
-100
-50
x
-550
-560
-570
-580
-590
-600

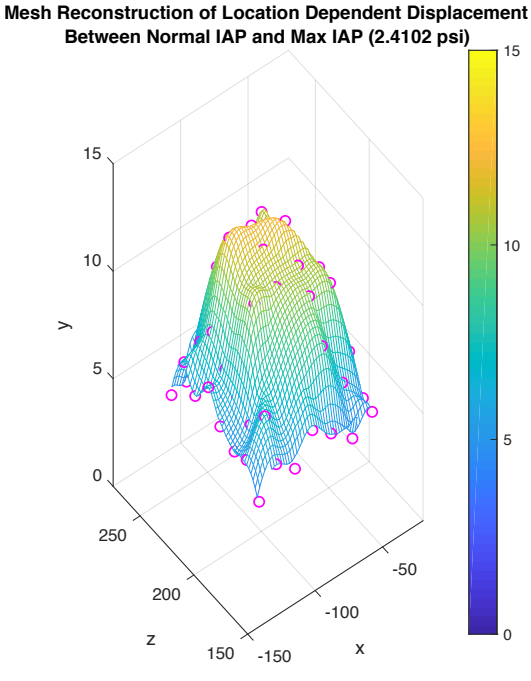
Mesh Reconstruction of Location Dependent Displacement
Between Normal IAP and Max IAP (2.4102 psi)
y
15
10
5
0
250
200
150
z
-150
-100
-50
x
15
10
5
0

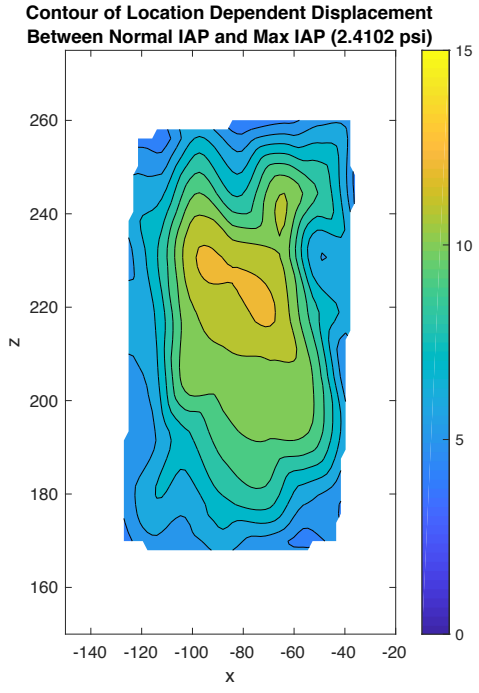
Contour of Location Dependent Displacement
Between Normal IAP and Max IAP (2.4102 psi)
z
260
240
220
200
180
160
-140
-120
-100
-80
-60
-40
-20
x
15
10
5
0

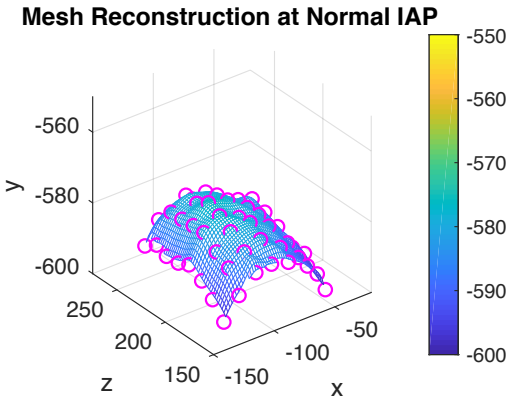
Mesh Reconstruction at Normal IAP
y
-560
-580
-600
z
250
200
150
x
-150
-100
-50
-550
-560
-570
-580
-590
-600

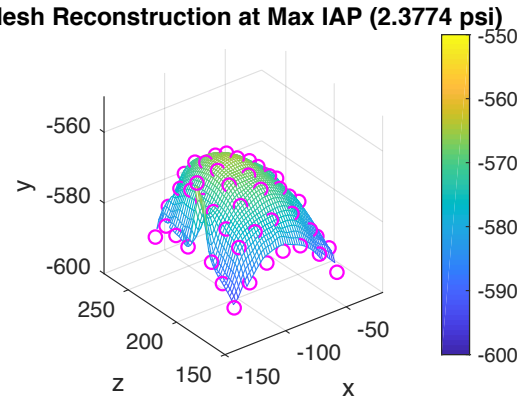
Mesh Reconstruction at Max IAP (2.3774 psi)
y
-560
-580
-600
z
250
200
150
x
-150
-100
-50
-550
-560
-570
-580
-590
-600

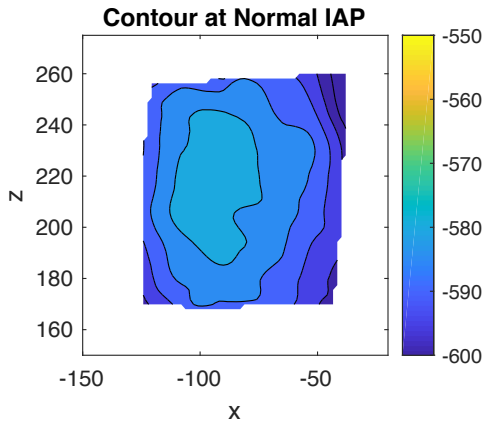
Contour at Normal IAP
z
260
240
220
200
180
160
x
-150
-100
-50
-550
-560
-570
-580
-590
-600

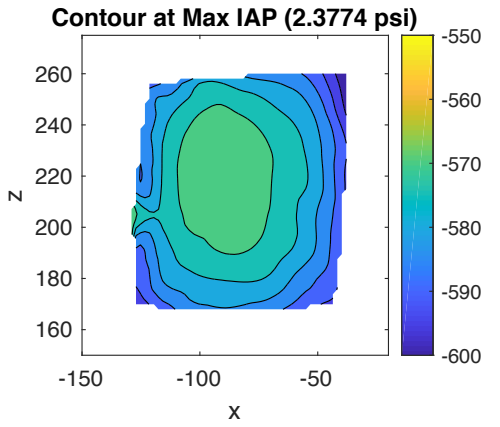
Contour at Max IAP (2.3774 psi)
z
260
240
220
200
180
160
x
-150
-100
-50
-550
-560
-570
-580
-590
-600

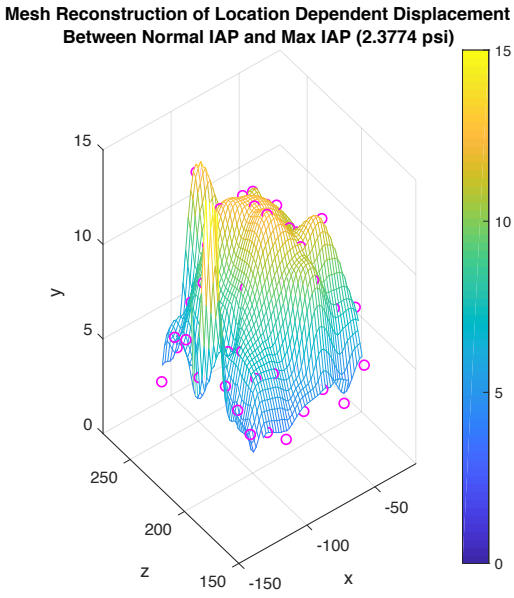
Mesh Reconstruction of Location Dependent Displacement
Between Normal IAP and Max IAP (2.3774 psi)
y
15
10
5
0
z
250
200
150
x
-150
-100
-50
15
10
5
0

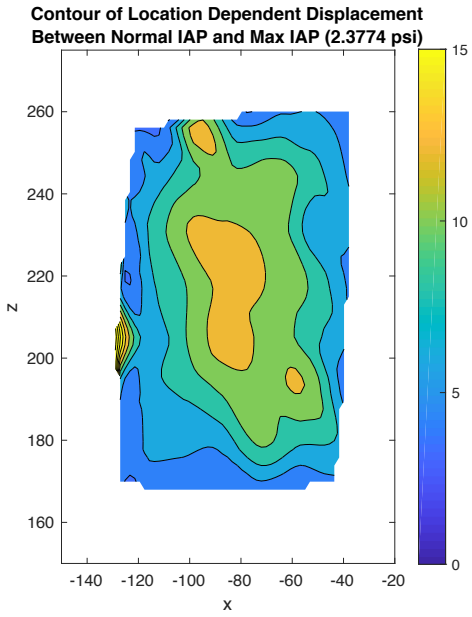
Contour of Location Dependent Displacement
Between Normal IAP and Max IAP (2.3774 psi)
z
260
240
220
200
180
160
x
-140
-120
-100
-80
-60
-40
-20
15
10
5
0

Appendix C: Mesh Reconstructions of Trials 7-9 (High Pressure Valve Closes at 2.2 psi)

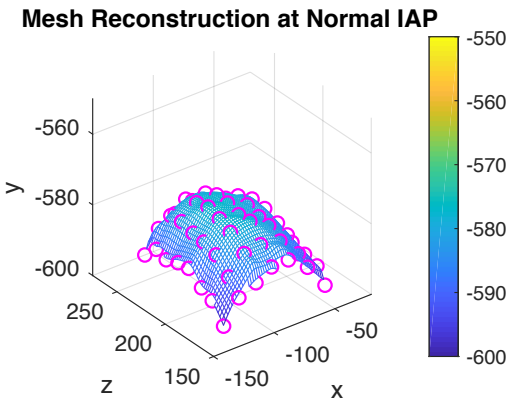

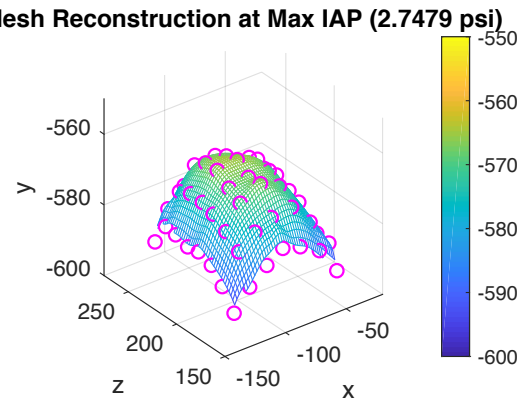

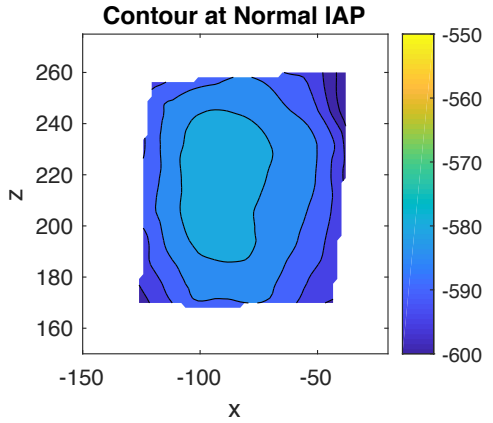

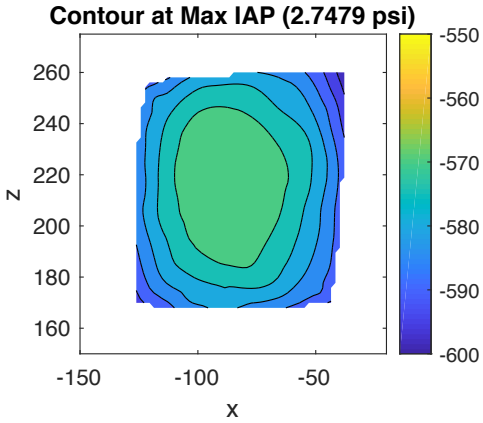

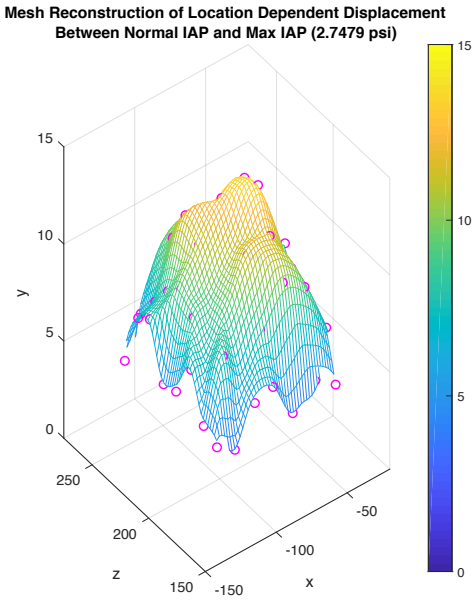

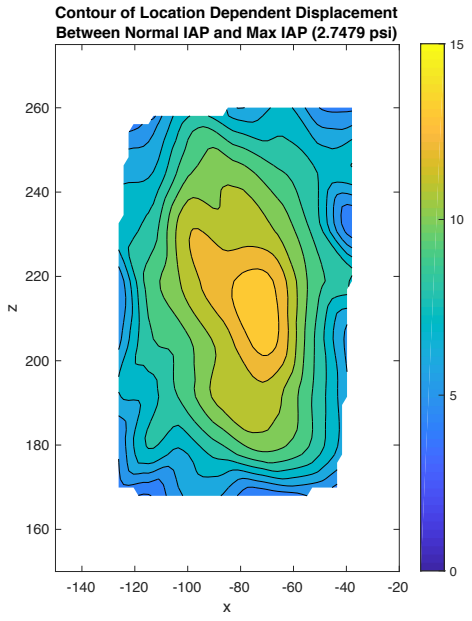

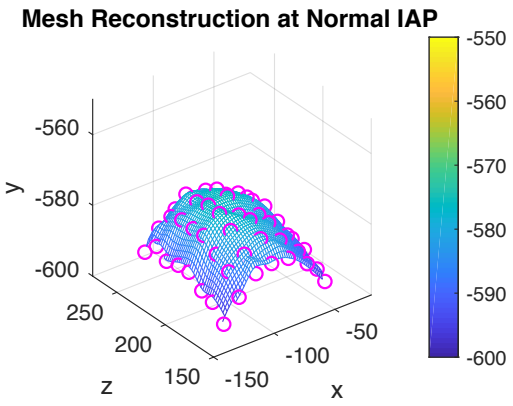
Mesh Reconstruction at Normal IAP
-560
-580
-600
y
250
200
150
z
-150
-100
-50
x
-550
-560
-570
-580
-590
-600

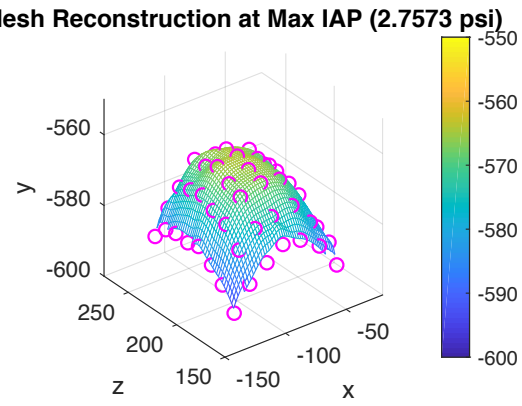
Mesh Reconstruction at Max IAP (2.7573 psi)
-560
-580
-600
y
250
200
150
z
-150
-100
-50
x
-550
-560
-570
-580
-590
-600

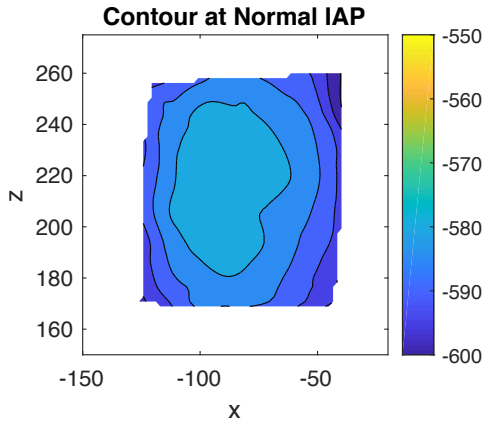
Contour at Normal IAP
260
240
220
200
180
160
z
-150
-100
-50
x
-550
-560
-570
-580
-590
-600

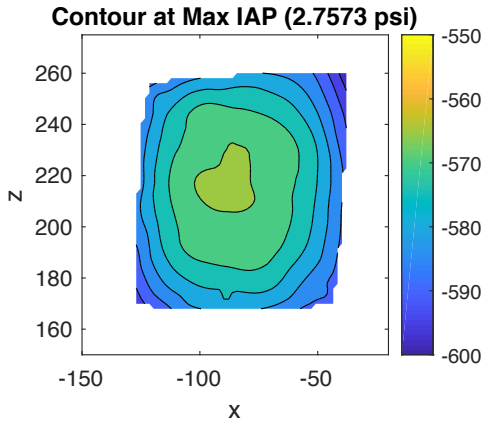
Contour at Max IAP (2.7573 psi)
260
240
220
200
180
160
z
-150
-100
-50
x
-550
-560
-570
-580
-590
-600

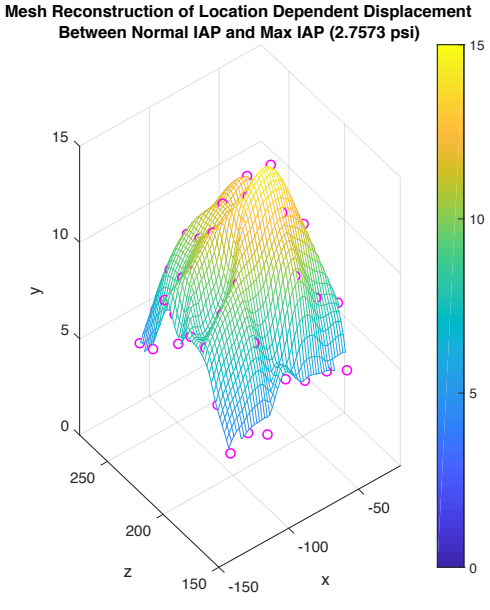
Mesh Reconstruction of Location Dependent Displacement
Between Normal IAP and Max IAP (2.7573 psi)
15
10
5
0
y
250
200
150
z
-150
-100
-50
x
15
10
5
0

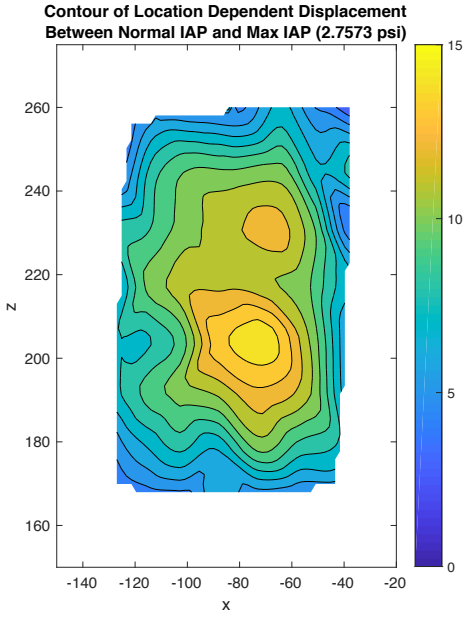
Contour of Location Dependent Displacement
Between Normal IAP and Max IAP (2.7573 psi)
260
240
220
200
180
160
z
-140
-120
-100
-80
-60
-40
-20
x
15
10
5
0

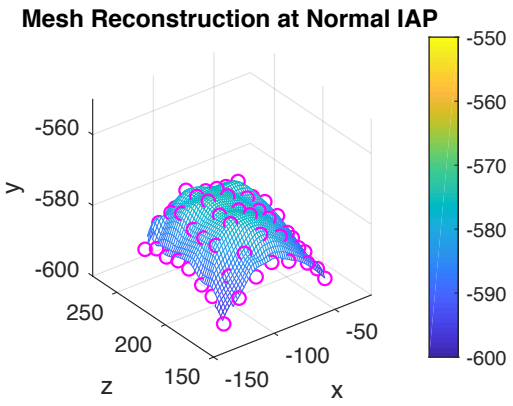
Mesh Reconstruction at Normal IAP
-560
-580
-600
y
250
200
150
z
-150
-100
-50
x
-550
-560
-570
-580
-590
-600

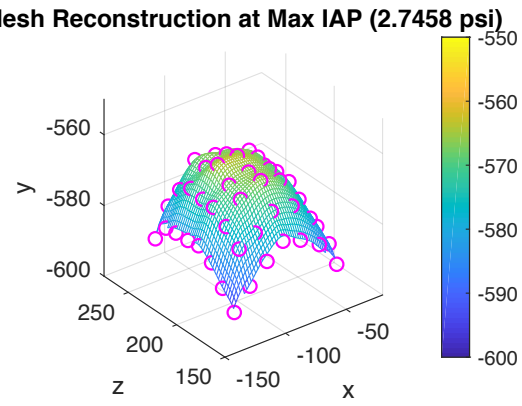
Mesh Reconstruction at Max IAP (2.7458 psi)
-560
-580
-600
y
250
200
150
z
-150
-100
-50
x
-550
-560
-570
-580
-590
-600

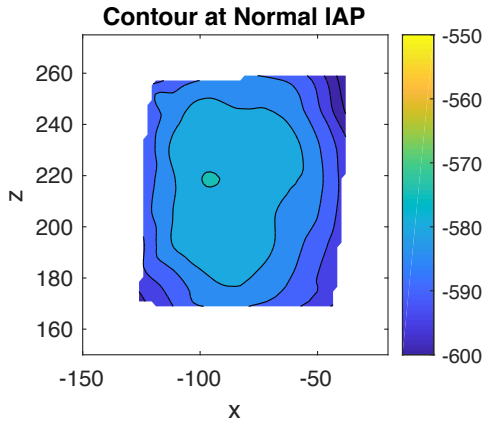
Contour at Normal IAP
260
240
220
200
180
160
z
-150
-100
-50
x
-550
-560
-570
-580
-590
-600

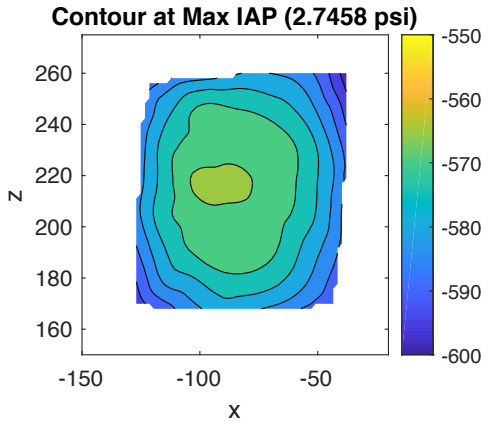
Contour at Max IAP (2.7458 psi)
260
240
220
200
180
160
z
-150
-100
-50
x
-550
-560
-570
-580
-590
-600

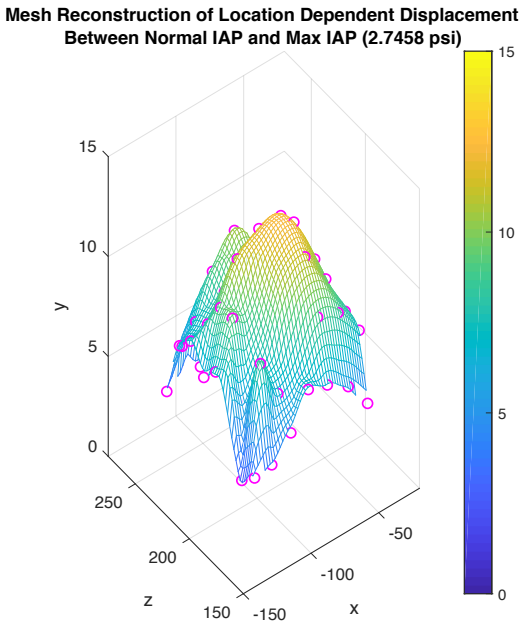
Mesh Reconstruction of Location Dependent Displacement
Between Normal IAP and Max IAP (2.7458 psi)
15
10
5
0
y
250
200
150
z
-150
-100
-50
x
15
10
5
0

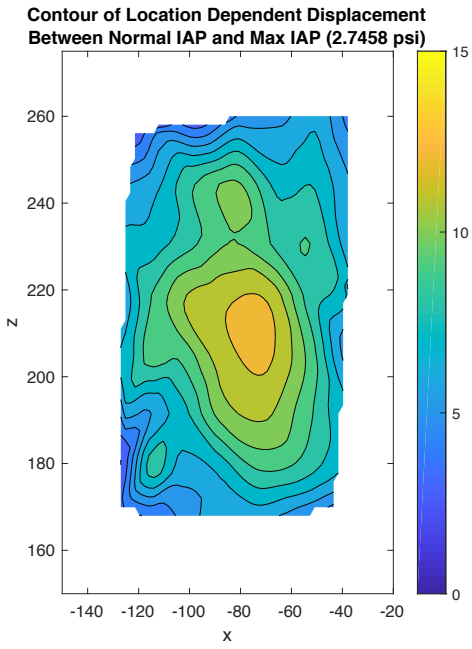
Contour of Location Dependent Displacement
Between Normal IAP and Max IAP (2.7458 psi)
260
240
220
200
180
160
z
-140
-120
-100
-80
-60
-40
-20
x
15
10
5
0

Appendix D: Mesh Reconstructions of Trials 10-12 (High Pressure Valve Closes at 2.6 psi)

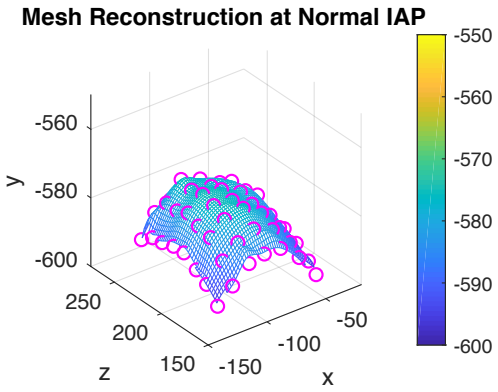

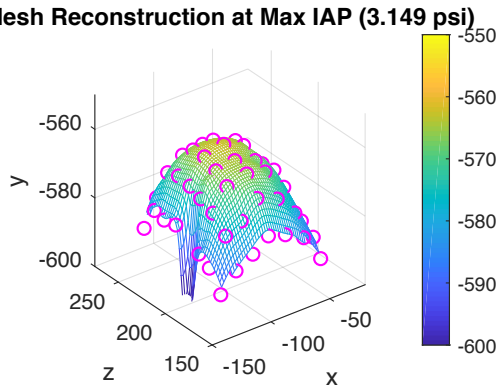

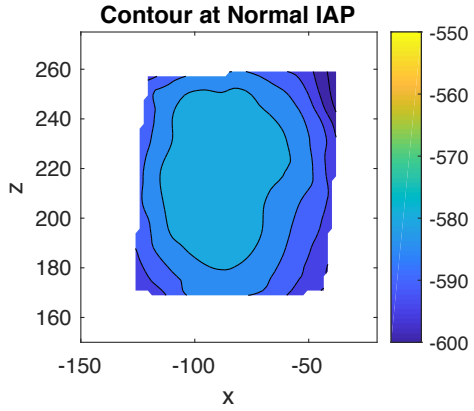

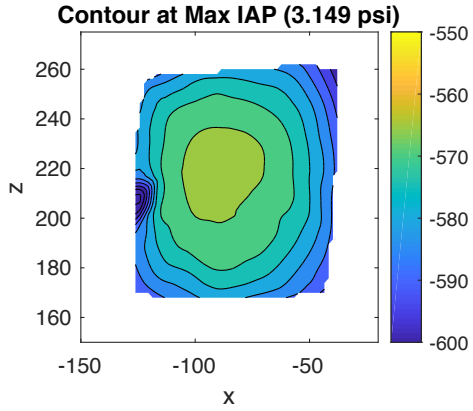

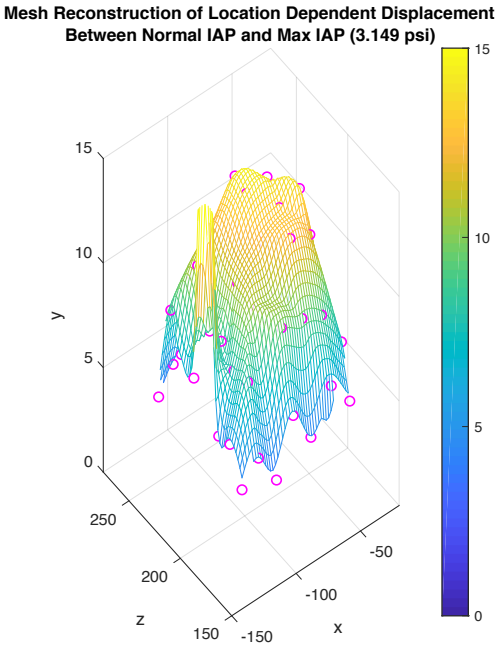

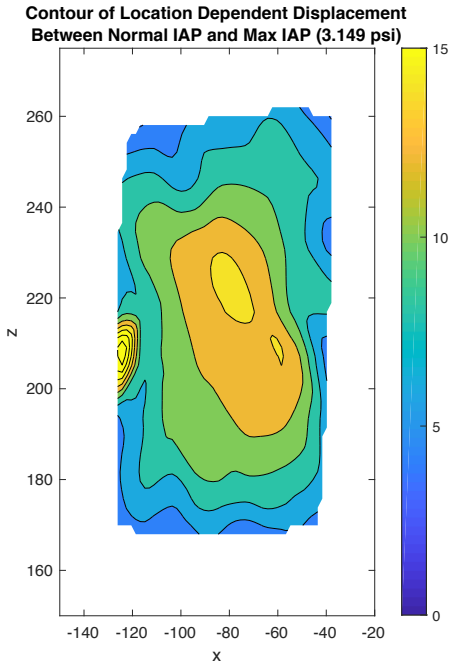

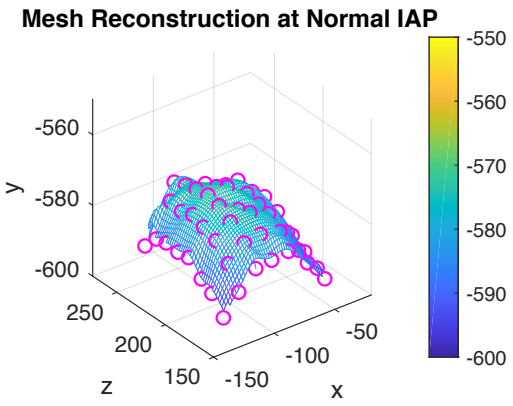
Mesh Reconstruction at Normal IAP
y
-560
-580
-600
z
250
200
150
x
-150
-100
-50
-550
-560
-570
-580
-590
-600

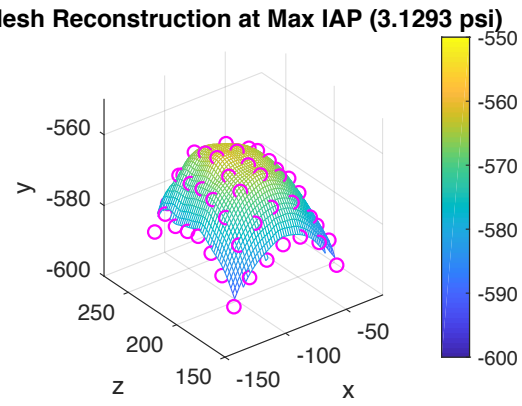
Mesh Reconstruction at Max IAP (3.1293 psi)
y
-560
-580
-600
z
250
200
150
x
-150
-100
-50
-550
-560
-570
-580
-590
-600

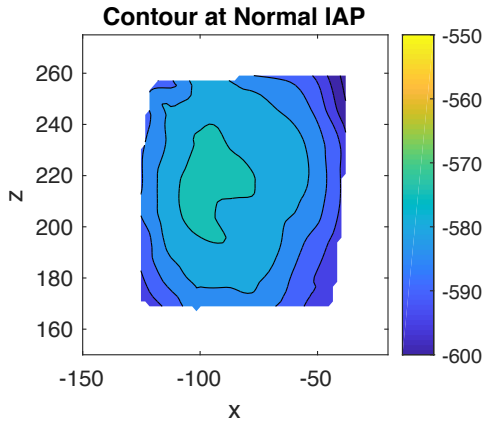
Contour at Normal IAP
z
260
240
220
200
180
160
x
-150
-100
-50
-550
-560
-570
-580
-590
-600

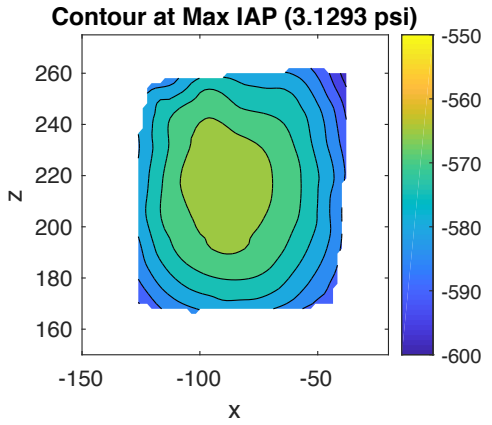
Contour at Max IAP (3.1293 psi)
z
260
240
220
200
180
160
x
-150
-100
-50
-550
-560
-570
-580
-590
-600

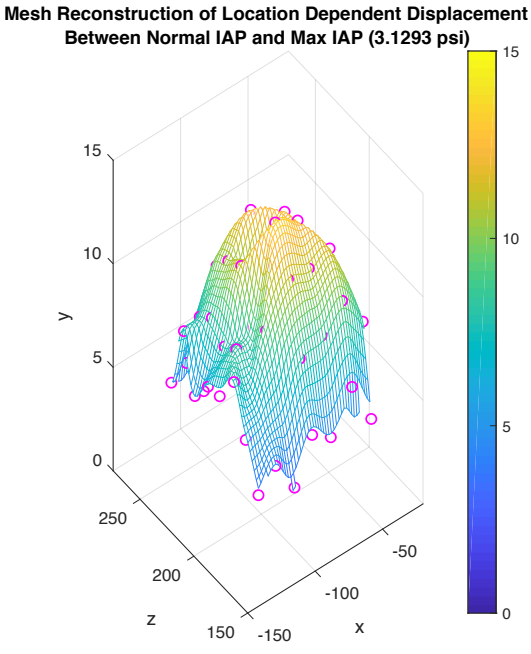
Mesh Reconstruction of Location Dependent Displacement
Between Normal IAP and Max IAP (3.1293 psi)
y
15
10
5
0
z
250
200
150
x
-150
-100
-50
15
10
5
0

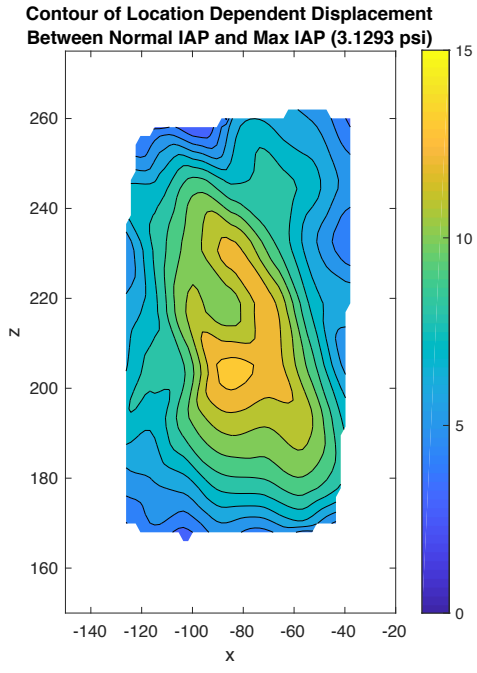
Contour of Location Dependent Displacement
Between Normal IAP and Max IAP (3.1293 psi)
z
260
240
220
200
180
160
x
-140
-120
-100
-80
-60
-40
-20
15
10
5
0

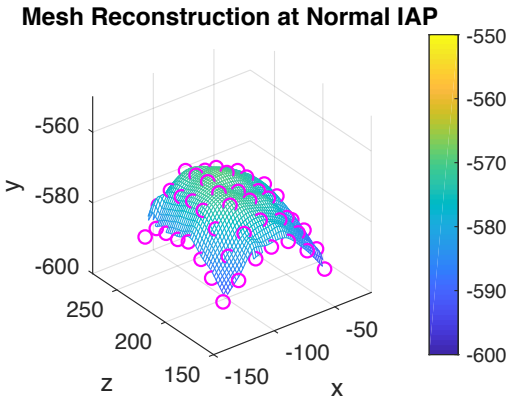
Mesh Reconstruction at Normal IAP
-560
-580
-600
y
250
200
150
z
-150
-100
-50
x
-550
-560
-570
-580
-590
-600

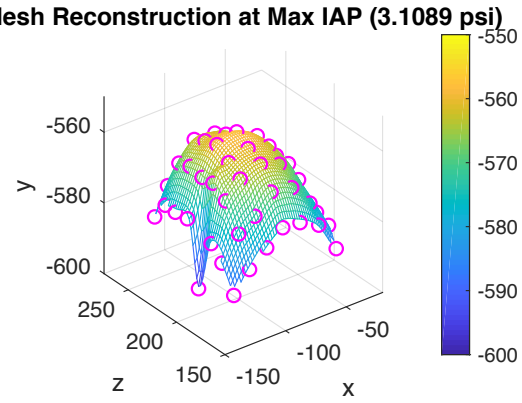
Mesh Reconstruction at Max IAP (3.1089 psi)
-560
-580
-600
y
250
200
150
z
-150
-100
-50
x
-550
-560
-570
-580
-590
-600

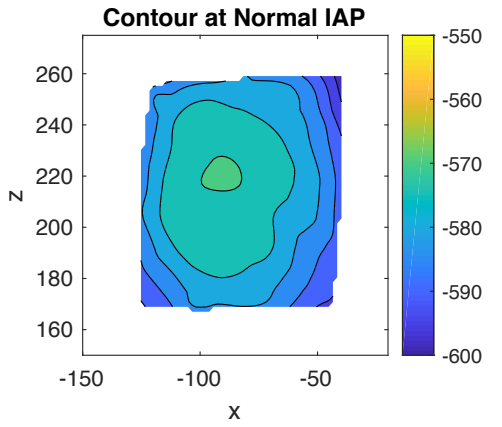
Contour at Normal IAP
260
240
220
200
180
160
z
-150
-100
-50
x
-550
-560
-570
-580
-590
-600

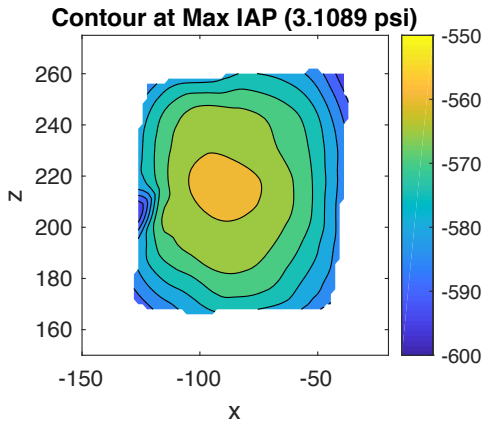
Contour at Max IAP (3.1089 psi)
260
240
220
200
180
160
z
-150
-100
-50
x
-550
-560
-570
-580
-590
-600

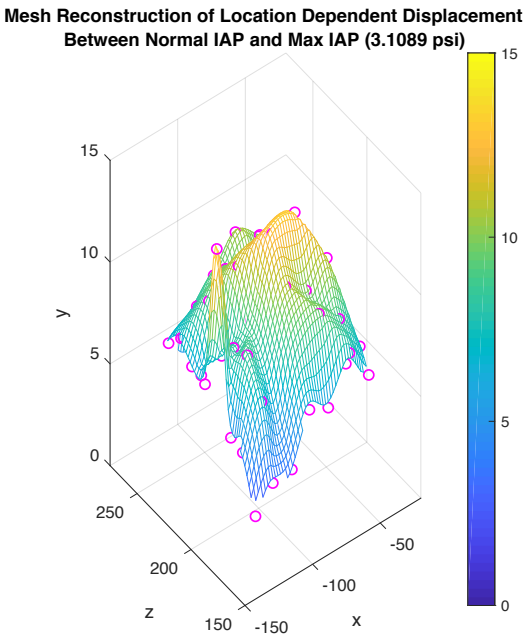
Mesh Reconstruction of Location Dependent Displacement
Between Normal IAP and Max IAP (3.1089 psi)
15
10
5
0
y
250
200
150
z
-150
-100
-50
x
15
10
5
0

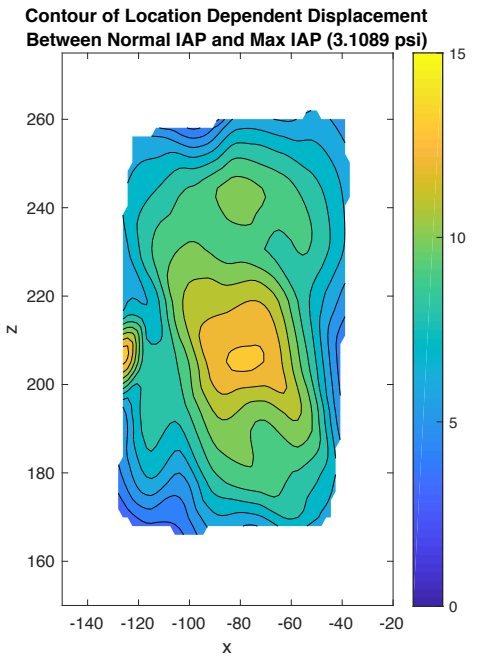
Contour of Location Dependent Displacement
Between Normal IAP and Max IAP (3.1089 psi)
260
240
220
200
180
160
z
-140
-120
-100
-80
-60
-40
-20
x
15
10
5
0